J|A|C|S
ARTICLES
Published on Web 03/26/2005

Substrate Oxidation by Copper−Dioxygen Adducts: Mechanistic Considerations

Jason Shearer,[†] Christiana Xin Zhang,[†] Lev N. Zakharov,[‡] Arnold L. Rheingold,[‡,¶] and Kenneth D. Karlin*[,†]

Contribution from the Department of Chemistry, Johns Hopkins University, 3400 North Charles Street, Baltimore, Maryland 21218, and Department of Chemistry, University of Delaware, Newark, Delaware 19716

Received August 9, 2004; E-mail: karlin@jhu.edu

Abstract: A series of copper−dioxygen adducts $[\{Cu^{II}(MePY2)^{R}\}_2(O_2)](B(C_6F_5)_4)_2$ (**1^{R}**), systematically varying in their electronic properties via ligand pyridyl donor substituents (R = H, MeO, and Me_2N), oxidize a variety of substrates with varying C−H or O−H bond dissociation enthalpies. Detailed mechanistic studies have been carried out, including investigation of **1^{R}** thermodynamic redox properties, **1^{R}** tetrahydrofuran (THF) and *N*,*N*′-dimethylaniline (DMA) oxidation kinetics (including analyses of substrate dicopper binding equilibria), and application of mechanistic probes (*N*-cyclopropyl-*N*-methylaniline (CMA) and (*p*-methoxyphenyl)-2,2-dimethylpropanol (MDP)), which can distinguish if proton-coupled electron-transfer (PCET) processes proceed through *concerted* electron-transfer proton-transfer (ETPT) *or consecutive* electron-transfer proton-transfer (ET/PT) pathways. The results are consistent with those of previous complementary studies; at low thermodynamic driving force for substrate oxidation, an ET/PT is operable, but once ET (i.e., substrate one-electron oxidation) becomes prohibitively uphill, the ETPT pathway occurs. Possible differences in coordination structures about **1^{Me_2N}**/**1^{MeO}** compared to those of **1^{H}** are also used to rationalize some of the observations.

Introduction

Copper-mediated oxidations are prominent in chemical and catalytic processes,[1−9] while tyrosinase (Tyr),[2,10] catechol oxidase (CO),[2,11] dopamine-β-hydroxylase (DBH),[3,12] and peptidylglycine α-hydroxylating monooxygenase (PHM)[13−15] are widely studied copper-containing monooxygenases/oxidases. Tyr and CO are structurally related, containing a peroxo-bridged magnetically coupled dinuclear Cu^{II}_2 active site (Scheme 1).[2,5,11] CO performs the catalytic conversion of *ortho*-catechols to *ortho*-quinones, while Tyr will both *ortho*-hydroxylate phenols and convert *ortho*-catechols to *ortho*-quinones (Scheme 1).[7,16] Tyr facilitates phenol hydroxylations by first coordinating a phenol (or phenolate) to one of the copper centers followed by an electrophilic attack of the phenol ring by the peroxo moiety.[2,10,17−19] In CO substrate dehydrogenation, concerted two-electron (two-proton) oxidation and radical-type proton-coupled electron-transfer (PCET) reaction mechanisms have been proposed.[1,11,20] DBH and PHM proceed through initial hydrogen atom ($H^{\bullet}$) abstraction reactions, which have been proposed to occur from either a mononuclear $Cu^{II}-O_2^{-\bullet}$ or a $Cu^{II}-OOH$ active-site oxidant.[12−15]

To aid in understanding the fundamental properties of the oxidative process in these metalloenzymes, as well as to potentially guide the design of oxidation reagents or catalysts, copper−dioxygen reactivity studies have received considerable attention.[7−9,21,22] The use of copper complexes and dioxygen in organic oxidations is well established,[22−27] but the emphasis

[†] Johns Hopkins University.
[‡] University of Delaware.
[¶] Current address: Chemistry Department, University of California, San Diego, La Jolla, CA 92093.

(1) Kitajima, N.; Moro-oka, Y. *Chem. Rev.* **1994**, *94*, 737−757.
(2) Solomon, E. I.; Sundaram, U. M.; Machonkin, T. E. *Chem. Rev.* **1996**, *96*, 2563−2605.
(3) Klinman, J. P. *Chem. Rev.* **1996**, *96*, 2541−2561.
(4) Kopf, M.-A.; Karlin, K. D. In *Biomimetic Oxidations*; Meunier, B., Ed.; Imperial College Press: London, 2000; Chapter 7, pp 309−362.
(5) Solomon, E. I.; Chen, P.; Metz, M.; Lee, S.-K.; Palmer, A. E. *Angew. Chem., Int. Ed.* **2001**, *40*, 4570−4590.
(6) Que, L., Jr.; Tolman, W. B. *Angew. Chem., Int. Ed.* **2002**, *41*, 1114−1137.
(7) Quant Hatcher, L.; Karlin, K. D. *J. Biol. Inorg. Chem.* **2004**, *9*, 669−683.
(8) Mirica, L. M.; Ottenwaelder, X.; Stack, T. D. P. *Chem. Rev.* **2004**, *104*, 1013−1045.
(9) Lewis, E. A.; Tolman, W. B. *Chem. Rev.* **2004**, *104*, 1047−1076.
(10) Decker, H.; Dillinger, R.; Tuczek, F. *Angew. Chem., Int. Ed.* **2000**, *39*, 1591−1595.
(11) Gerdemann, C.; Eicken, C.; Krebs, B. *Acc. Chem. Res.* **2002**, *35*, 183−191.
(12) Evans, J. P.; Ahn, K.; Klinman, J. P. *J. Biol. Chem.* **2003**, *278*, 49691−49698.
(13) Chen, P.; Bell, J.; Eipper, B. A.; Solomon, E. I. *Biochemistry* **2004**, *43*, 5735−5747.
(14) (a) Chen, P.; Solomon, E. I. *J. Am Chem. Soc.* **2004**, *126*, 4991−5000. (b) Chen, P.; Solomon, E. I. *Proc. Natl. Acad. Sci. U.S.A.* **2004**, *101*, 13105−13110.
(15) Prigge, S. T.; Eipper, B.; Mains, R.; Amzel, L. M. *Science* **2004**, *304*, 864−867.
(16) Sanchez-Ferrer, A.; Rodriguez-Lopez, J. N.; Garcia-Canovas, F.; Garcia-Carmona, F. *Biochim. Biophys. Acta* **1995**, *1247*, 1−11.
(17) Pidcock, E.; Obias, H. V.; Zhang, C. X.; Karlin, K. D.; Solomon, E. I. *J. Am. Chem. Soc.* **1998**, *120*, 7841−7847.
(18) Itoh, S.; Kumei, H.; Taki, M.; Nagatomo, S.; Kitagawa, T.; Fukuzumi, S. *J. Am. Chem. Soc.* **2001**, *123*, 6708−6709.
(19) Yamazaki, S.-i.; Itoh, S. *J. Am Chem. Soc.* **2003**, *125*, 13034−13035.
(20) Klabunde, T.; Eicken, C.; Sacchettini, J. C.; Krebs, B. *Nat. Struct. Biol.* **1998**, *5*, 1084−1090.
(21) Stack, T. D. P. *Dalton Trans.* **2003**, 1881−1889.
(22) Karlin, K. D.; Gultneh, Y. *Prog. Inorg. Chem.* **1987**, *35*, 219−327.

Scheme 1

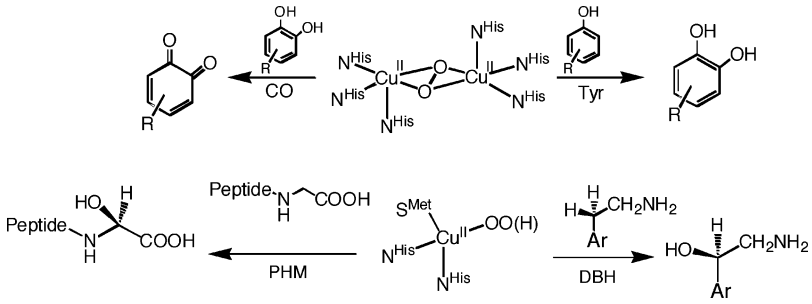

on detailed mechanistic studies employing discrete copper−dioxygen adducts is more recent.[7,9] Oxidative N-dealkylation reactions of copper ligands are common,[9] with those involving *intra*molecular ligand oxidations of Cu^{III}_2−bis-μ-oxo complexes by far being the best represented.[28−31] From both theoretical[32,33] and experimental (kinetic) arguments,[28−31] it has been suggested that such reactions occur through an initial rate-limiting *concerted* proton-coupled electron-transfer (PCET) reaction (an ETPT reaction, often referred to as hydrogen atom abstraction (HAT), Scheme 2), as opposed to a *consecutively* occurring PCET (an ET/PT reaction, Scheme 2).[34,35]

Scheme 2

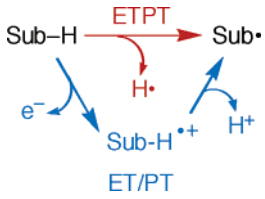

*Inter*molecular exogenous substrate oxidations by Cu_2−O_2 species are less well documented.[18,30,36−38] In studies by Itoh, it has been suggested that both Cu^{II}_2−(η^2:η^2-μ-peroxo) and Cu^{III}_2−bis-μ-oxo complexes oxidize phenols (to coupled phenol dimers) through ET/PT-type pathways.[39] Furthermore, for both phenolate oxygenation by a Cu^{II}_2−(η^2:η^2-μ-peroxo) complex to give *o*-catechols[40] and phenol oxidation promoted by a trinuclear Cu−dioxygen species,[41] it is suggested that substrate coordination to the metal center is important for subsequent substrate oxidative transformations.

Recently, we reported the synthesis, properties, and reactivity of a series of $Cu_2(O_2)$ complexes, $[\{Cu^{II}(MePY2)^R\}_2(O_2^{2-})]^{2+}$ (R = H, MeO, and Me_2N, $\mathbf{1^R}$; Scheme 3), that contain copper

Scheme 3

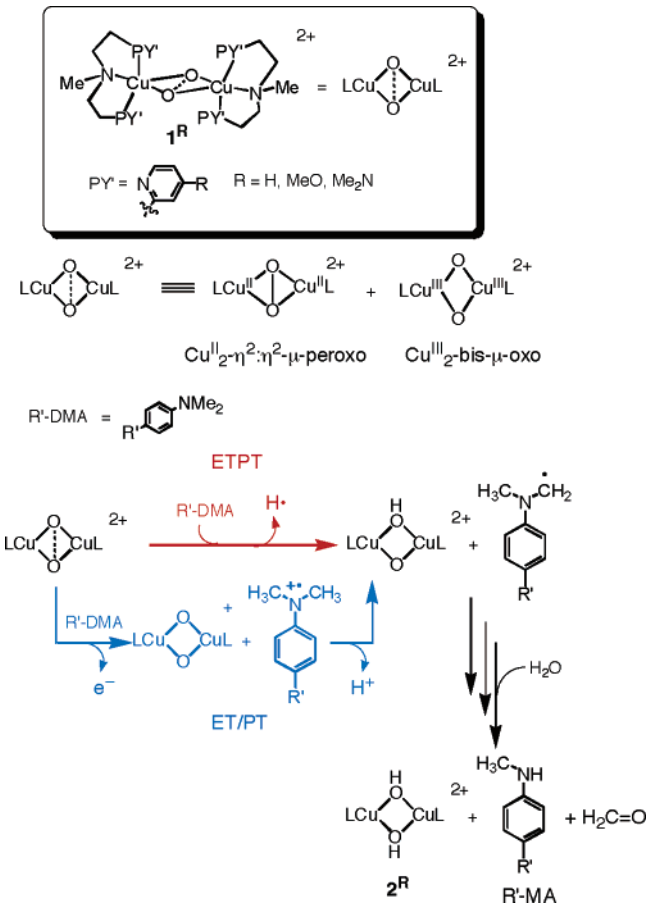

ligated by *para*-substituted bispyridyl(ethylamine) ligands, $(MePY2)^R$.[42−44] These complexes are capable of oxidizing a variety of substrates in good yields, making them excellent

(23) *Oxidation in Organic Chemistry*; Trahanovsky, W. S., Ed.; Academic Press: New York, 1973; Vol. Part B, Chapter 1.
(24) Sprecher, C. A.; Zuberbühler, A. D. *Angew. Chem., Int. Ed. Engl.* **1977**, *16*, 189.
(25) Gampp, H.; Zuberbühler, A. D. *Met. Ions Biol. Syst.* **1981**, *12*, 133−189.
(26) Zuberbühler, A. D. In *Copper Coordination Chemistry: Biochemical and Inorganic Perspectives*; Karlin, K. D., Zubieta, J., Eds.; Adenine: Guilderland, NY, 1983; pp 237−258.
(27) Reglier, M.; Amadei, E.; Alilou, E. H.; Eydoux, F.; Pierrot, M.; Waegell, B. *Bioinorg. Chem. Copper* **1993**, 348−362.
(28) Mahapatra, S.; Young, V. G., Jr.; Kaderli, S.; Zuberbühler, A. D.; Tolman, W. B. *Angew. Chem., Int. Ed. Engl.* **1997**, *36*, 130−133.
(29) Mahadevan, V.; Hou, Z.; Cole, A. P.; Root, D. E.; Lal, T. K.; Solomon, E. I.; Stack, T. D. P. *J. Am. Chem. Soc.* **1997**, *119*, 11996−11997.
(30) Taki, M.; Itoh, S.; Fukuzumi, S. *J. Am. Chem. Soc.* **2001**, *123*, 6203−6204.
(31) Mahapatra, S.; Halfen, J. A.; Tolman, W. B. *J. Am. Chem. Soc.* **1996**, *118*, 11575−11586.
(32) Cramer, C. J.; Kinsinger, C. R.; Pak, Y. *THEOCHEM* **2003**, *632*, 111−120.
(33) Cramer, C. J.; Pak, Y. *Theor. Chem. Acc.* **2001**, *105*, 477−480.
(34) Cukier, R. I. *J. Phys. Chem. B* **2002**, *106*, 10089−10100.
(35) Since the specifics of these reactions are unknown from a theoretical standpoint (i.e., we do not know if the electron and proton are going to the same (a hydrogen atom transfer (HAT)) or different (a concerted PCET) acceptor orbitals), we prefer to use Cukier's more general nomenclature (ref 34) for thermodynamically coupled proton/electron-transfer reactions. Here, "ETPT" means that the ET and PT occur in one kinetically irresolvable step, while "ET/PT" designates that the ET and PT processes can be broken down into two kinetically resolvable steps, with the ET event occurring prior to proton transfer (PT).
(36) Fukuzumi, S.; Ohtsu, H.; Ohkubo, K.; Itoh, S.; Imahori, H. *Coord. Chem. Rev.* **2002**, *226*, 71−80.
(37) Mahadevan, V.; Henson, M. J.; Solomon, E. I.; Stack, T. D. P. *J. Am. Chem. Soc.* **2000**, *122*, 10249−10250.
(38) Mahadevan, V.; DuBois, J. L.; Hedman, B.; Hodgson, K. O.; Stack, T. D. P. *J. Am. Chem. Soc.* **1999**, *121*, 5583−5584.
(39) Osako, T.; Ohkubo, K.; Taki, M.; Tachi, Y.; Fukuzumi, S.; Itoh, S. *J. Am. Chem. Soc.* **2003**, *125*, 11027−11033.
(40) Itoh, S.; Kumei, H.; Nagatomo, S.; Kitagawa, T.; Fukuzumi, S. *J. Am. Chem. Soc.* **2001**, *123*, 2165−2175.
(41) Taki, M.; Teramae, S.; Nagatomo, S.; Tachi, Y.; Kitagawa, T.; Itoh, S.; Fukuzumi, S. *J. Am. Chem. Soc.* **2002**, *124*, 6367−6377.

candidates for detailed mechanistic studies of Cu_2-O_2-mediated exogenous substrate oxidations.[42] An initial study was published concerning PCET reactions between $\mathbf{1^R}$ and *para*-substituted *N*,*N*-dimethylanilines (R′-DMAs), which undergo N-dealkylations yielding $[\{Cu^{II}(MePY2)^R\}_2(OH)_2]^{2+}$ ($\mathbf{2^R}$), *para*-substituted methylanilines, and formaldehyde (Scheme 3).[44] On the basis of linear-free energy and deuterium kinetic isotope effect (KIE) studies, we determined that both ET/PT *and* ETPT pathways are possible for these oxidations, with ET being rate limiting in the ET/PT case. For $\mathbf{1^H}$, we suggested that all R′-DMA oxidations occurred through an ET/PT pathway, while there was a switch-over in the mechanism for R′-DMA oxidation by $\mathbf{1^{MeO}}$ and $\mathbf{1^{Me_2N}}$. Since the R′-DMA substrate is made more difficult to oxidize by one electron, the mechanism changes from ET/PT to ETPT.

In the present study, we disclose a much more detailed investigation on the mechanism of PCET reactions facilitated by $\mathbf{1^R}$. Given that both KIEs and linear free-energy correlations can be difficult to interpret, we decided to further explore the nature of PCET reactions by $\mathbf{1^R}$ (i.e., ETPT versus ET/PT) using two mechanistic probes. Mechanistic probes are substrates that give unambiguous and different products depending on reaction pathways. The probes chosen for this study are *N*-cyclopropyl-*N*-methylaniline (CMA)[45] and (*p*-methoxyphenyl)-2,2-dimethylpropanol (MDP).[46] Here, the differential stabilities of radical ($H^\bullet$ loss) versus radical cation (e^- loss) intermediates formed following initial probe oxidation can allow us to differentiate between reaction pathways. To delineate the scope of $\mathbf{1^R}$ reactivity, we also present the reaction patterns of $\mathbf{1^R}$ toward substrates possessing both similar (i.e., 2,5-dimethyltetrahydrofuran (Me_2THF), toluene, diethyl ether (Et_2O)) *and* significantly weaker bond dissociation enthalpies (BDEs) (i.e., 9,10-dihydroanthracene (DHA) and 2,2,6,6-tetramethylpiperidin-1-ol (TEMPO-H)) compared to those of DMAs. Electrochemical and thermodynamic information for the $\mathbf{1^R}$ series is also presented to further aid us in gaining mechanistic insight for these oxidations. Furthermore, evidence for a pre-equilibrium involving substrate coordination to the metal center prior to oxidation is provided. Overall, the present study provides not only new insights but also a more detailed mechanistic picture concerning the mechanism of substrate oxidations by copper−dioxygen adducts.

Experimental Section

General Methods. All reactions were performed under an atmosphere of argon using standard Schlenk techniques. Cu^I complexes, $[Cu^I(MePY2)^H]B(C_6F_5)_4$, $[Cu^I(MePY2)^{MeO}]B(C_6F_5)_4$, and $[Cu^I(MePY2)^{Me_2N}]B(C_6F_5)_4$, were prepared according to previously published procedures.[42,44] Mechanistic probes, *N*-methyl-*N*-cyclopropylaniline (CMA),[47] (*p*-methoxyphenyl)-2,2-dimethylpropanol (MDP),[48] and TEMPO-H,[49] as well as cyclopropylaniline (CA),[50] (*p*-methoxyphenyl)-2,2-dimethylpropanone (MDK),[51] and *N*-methylquinolinium (MQ^+) sulfate,[52] were all prepared through literature methods. $NH_4(B(C_6F_5)_4)$ and $NBu_4(B(C_6F_5)_4)$ were prepared by the method of Geiger; NR_4Br underwent a metathesis reaction with $Li(B(C_6F_5)_4)\cdot Et_2O$ (Boulder Scientific, Boulder, CO) in $EtOH/H_2O$.[53] Ferrocene, dimethylferrocene, ethylferrocene, decamethylferrocene, $[Fe^{II}(phen)_2(phen\text{-}NO_2)](ClO_4)_2$, *N*-methylaniline (MA), *para*-methoxybenzaldehyde (BA), 9,10-dihydroanthracene (DHA), and *N*,*N*-dimethylaniline (DMA) were all obtained through commercial sources and purified prior to use according to standard procedures.[54] Solvents were purified using a commercially available double alumina column solvent purification system (Innovative Technologies, Inc.) and were degassed prior to use. All other reagents were used as received. Electronic absorption spectra were recorded on a Hewlett-Packard 8453 UV−vis spectrometer in a quartz optical Dewar using Schlenk cuvettes with a 1 cm path length. The methanol bath inside the Dewar was maintained at the desired temperature (within ±0.1 °C) by cooling with a Neslab ULT-95 low-temperature circulating cooler. NMR spectra were recorded on a Bruker AMX 300 FTNMR spectrometer. EPR spectra were recorded in quartz EPR tubes on a Bruker EMX CWEPR spectrometer. The cavity was maintained at 65 K with the use of a He cryostat. Stopped-flow kinetic traces were recorded on a Hi-Tech SF-40 variable-temperature stopped-flow unit (1 × 0.2 cm quartz cell) equipped with a J&M-Tidas spectrometer.

***N*,*N*-Dimethylaniline and Tetrahydrofuran (DMA and THF) Reaction Kinetic Analysis.** Solutions of $[\{Cu^{II}(MePY2)^R\}_2(O_2)](B(C_6F_5)_4)_2$ ($\mathbf{1^R}$) in CH_2Cl_2 ($[\mathbf{1^R}]$ ranged between 4.0×10^{-5} and 6.5×10^{-5} M) were prepared by bubbling solutions of $[Cu^I(MePY2)^R]B(C_6F_5)$ in CH_2Cl_2 with dioxygen at low temperatures (−85 to −65 °C). UV−vis reaction monitoring was carried out using an apparatus with a quartz cuvette at one end of a long (14 in.) glass tube and air-free handling stopcocks and ground-glass joints at the other of which 10 in. is completely immersed in a cold methanol bath. After complete formation of $\mathbf{1^R}$, as noted by the Abs at 355 nm (or 360 nm for $\mathbf{1^{Me_2N}}$), the solutions were purged of excess dioxygen with argon. A solution of DMA (500 μL) in CH_2Cl_2 was then *slowly* layered over the top of the reaction mixture by adding it down the side of the tube so that no solution mixing was obtained. After a brief period to allow for temperature equilibration, the reaction was initiated by mixing the solutions together with a gentle stream of argon, and then the reaction was monitored by UV−vis spectroscopy. For the higher-temperature reactions (−80 to −65 °C) involving DMA and $\mathbf{1^{Me_2N}}$, stopped-flow methods were used to follow the course of the reaction. Here, an O_2-saturated solution of CH_2Cl_2 was injected into a CH_2Cl_2 solution of $[Cu^I(MePY2)^{Me_2N}]B(C_6F_5)$ and DMA, and the reaction was monitored. First-order rate constants for all DMA oxidation reactions were then extracted either manually using the change in Abs at 355 nm (360 nm for $\mathbf{1^{Me_2N}}$) or automatically using either SpecFit/32 (Spectrum Software Associates, Marborough, MA)[55] or an in-house series of procedures written for Igor Pro 4.0 (Wavemetrics, Lake Oswego, OR). All three methods gave identical first-order rate constants (k_{obs}). Data were collected at several different DMA concentrations (0.8−30 mM) over the temperature range of −65 to −85 °C. Plots of k_{obs}^{-1} versus $[DMA]^{-1}$ were then fit to a Lineweaver−Burk-type plot (eq 1):

$$k_{obs}^{-1} = k_{ox}^{-1} + (K_{eq}k_{ox})^{-1}[DMA]^{-1} \quad (1)$$

(42) (a) Zhang, C. X.; Liang, H.-C.; Kim, E.-i.; Shearer, J.; Helton, M. E.; Kim, E.; Kaderli, S.; Incarvito, C. D.; Zuberbühler, A. D.; Rheingold, A. L.; Karlin, K. D. *J. Am Chem. Soc.* **2003**, *125*, 634−635. (b) Liang, H.-C.; Karlin, K. D.; Dyson, R.; Kaderli, S.; Jung, B.; Zuberbühler, A. D. *Inorg. Chem.* **2000**, *39*, 5884−5894.

(43) Henson, M. J.; Vance, M. A.; Zhang, C. X.; Liang, H.-C.; Karlin, K. D.; Solomon, E. I. *J. Am. Chem. Soc.* **2003**, *125*, 5186−5192.

(44) Shearer, J.; Zhang, C. X.; Hatcher, L. Q.; Karlin, K. D. *J. Am. Chem. Soc.* **2003**, *125*, 12670−12671.

(45) Shaffer, C. L.; Harriman, S.; Koen, Y. M.; Hanzlik, R. P. *J. Am. Chem. Soc.* **2002**, *124*, 8268−8274.

(46) Baciocchi, E.; Bietti, M.; Lanzalunga, O. *Acc. Chem. Res.* **2000**, *33*, 243−251.

(47) Shaffer, C. L.; Morton, M. D.; Hanzlik, R. P. *J. Am. Chem. Soc.* **2001**, *123*, 349−350.

(48) Baciocchi, E.; Bietti, M.; Putignani, L.; Steenken, S. *J. Am. Chem. Soc.* **1996**, *118*, 5952−5960.

(49) Mader, E. A.; Larsen, A. S.; Mayer, J. M. *J. Am. Chem. Soc.* **2004**, *126*, 8066−8067.

(50) Cui, W.; Loeppky, R. N. *Tetrahedron* **2001**, *57*, 2953−2956.

(51) Smyth, T. P.; Corby, B. W. *J. Org. Chem.* **1998**, *63*, 8946−8951.

(52) Hammond, P. R. U.S. Patent Appl. 566,924, November 9, 1984.

(53) LeSuer, R. J.; Geiger, W. E. *Angew. Chem., Int. Ed.* **2000**, *39*, 248−250.

(54) Armarego, C. *Purification of Laboratory Chemicals*, 5th ed.; Butterworth Heinemann: New York, 2003.

(55) Gampp, H.; Maeder, M.; Meyer, C. J.; Zuberbühler, A. D. *Talanta* **1985**, *32*, 95−110.

Table 1. Product Yields in the Oxidation of Mechanistic Probes CMA and MDP (see Schemes 7, 8, and 10) by $\mathbf{1^R}$ in CH_2Cl_2 at −80 °C as Assessed by GC/MS Analysis

	$\mathbf{1^H}$ (%)	$\mathbf{1^{MeO}}$ (%)	$\mathbf{1^{Me_2N}}$ (%)
Oxidation of CMA			
PMA[a]	20(5)	30(5)	<0.1[c]
MA	48(2)	55(1)	2(1)
CA	6(1)	2(1)	2(1)
MQ^+	<0.1[c]	<0.1[c]	50(20)[d]
total yield of CMA[b]	74	88	50−100[e]
Oxidation of MDP			
MDK	10(3)	47(3)	63(8)
MBA	31(2)	< 0.1[c]	<0.1[c]
total yield of MDP[b]	41	47	63

[a] Product yields of PMA were calculated by comparison to the peak area of MA (see Schemes 7 and 10, and the Experimental Section). [b] Total yields are based on the amount of product quantified by GC analysis. [c] No product was detected by GC. [d] Based upon gravimetric analysis of the isolated product. [e] See text for details.

where k_{ox} is the oxidation rate constant, and K_{eq} is the equilibrium constant for DMA binding to $\mathbf{1^R}$.[18] Rate constants for THF oxidation by $\mathbf{1^{Me_2N}}$ were determined in a similar manner using both stopped-flow and benchtop UV−vis methods over the temperature range of −90 to −70 °C. Here, the THF concentration in CH_2Cl_2 was varied between 0.1 and 2.0 M. First-order rate constants (k_{obs}) were extracted as mentioned above and plotted versus THF concentration. The slope of this fit was then taken as the second-order rate constant, k_{ox}. Activation and thermodynamic parameters were then obtained using van't Hoff or Eyring plots.[56]

Mechanistic Probe (CMA and MDP, see Schemes 7 and 8) Oxidation Reactions and Product Analysis (Table 1). In a typical reaction, 50 mg of $[Cu^I(MePY2)^R](B(C_6F_5)_4)$ was dissolved in 2 mL of CH_2Cl_2 and cooled in a dry ice/acetone bath to −78 °C. Dioxygen was then slowly bubbled through the reaction mixture for ∼30 s and then through the reaction headspace for an additional 120 s. After full formation of $[\{Cu^{II}(MePY2)^R\}_2(O_2)](B(C_6F_5)_4)_2$ ($\mathbf{1^R}$) was obtained (2−30 min), the reaction mixtures were then purged with argon to remove all residual dioxygen. Ten equivalents of substrate CMA or MDP and 1 equiv of decane were dissolved in 500 μL of argon-sparged CH_2Cl_2 and then injected into the reaction mixture. The reaction mixture was then placed in a low-temperature freezer (−80 °C) for 24 h to 7 days. By this time, the reaction went to completion as noted by full formation of $[\{Cu^{II}(MePY2)^R\}_2(OH)_2](B(C_6F_5)_4)_2$ ($\mathbf{2^R}$). The reaction mixture was then passed through a short plug of alumina to remove all $\mathbf{2^R}$. All reaction mixtures were then analyzed by GC/MS on a Shimadzu GCMS-QP5050A equipped with a DB-5M5 packed J&W Scientific (30 m/0.25 mm i.d.) column. Quantification of yields was then determined by standard calibration curves of decane versus the various products. Due to the unstable nature of *ortho*-(propan-3-al)-*N*-methylaniline, a calibration curve could not be constructed using authentic sample; therefore, we had to estimate yields of this product by integration relative to *N*-methylaniline. The reaction between $\mathbf{1^{Me_2N}}$ and CMA produced *N*-methylquinolinium (MQ^+), which was isolated by column chromatography of the reaction mixture (alumina). The resulting solution was evaporated to dryness and weighed on an analytical balance. The ^{1}H NMR spectrum of the product was then compared to the ^{1}H NMR spectrum of an authentic sample of MQ^+ and found to be nearly identical (see Discussion and Supporting Information, Figure S15). All results represent the average of three separate experiments.

Exogenous Substrate Oxidation. The oxidation of exogenous substrates was monitored in two ways. First, we monitored the decay of $\mathbf{1^R}$ by UV−vis (−80 °C) in 0.5 M CH_2Cl_2 solutions of substrate (TEMPO-H, toluene, DHA, Et_2O, Me_2THF) by noting the loss of the band at 355 nm (360 nm for $\mathbf{1^{Me_2N}}$). The first-order oxidation rate was then extracted and compared to the decay of $\mathbf{1^R}$ in the absence of substrate ($k < 10^{-6}$ s^{-1}). If the rate of oxidation in the presence of substrate was comparable to that in the absence of substrate, it was concluded that $\mathbf{1^R}$ did not react with that substrate. We also examined the oxidation of substrate on a "synthetic" scale using a procedure identical to that used for mechanistic probe oxidations. Products were then analyzed by GC/MS. For the case of diethyl ether oxidation, we noted oxidation was taking place; however, GC/MS revealed no identifiable products. Therefore, we used Fehling's test ($CuSO_4$/Rochell's salt) to confirm the presence of an aldehyde.[57]

Electrochemical Measurements and Spectroelectrochemical Titrations. Cyclic voltammograms (CVs) were obtained at −78 °C in a dry ice/acetone bath and recorded with a BAS-100B potentiostat interfaced to a personal computer. To aid in data quality of the CV waves and subsequent data analysis, CVs were recorded in 5 mV (as opposed to 1 mV) increments. All measurements were recorded in a Faraday cage, using $Bu_4N(B(C_6F_5)_4)$ (0.1 M) as the supporting electrolyte in CH_2Cl_2. In a typical experiment, a 0.01 M solution of the Cu^I complex was exposed to dioxygen (resulting in 0.005 M $\mathbf{1^R}$) and then purged with argon after full formation of $\mathbf{1^R}$ was noted. For $\mathbf{1^H}$ and $\mathbf{1^{MeO}}$, a standard three-electrode cell was used containing a glassy carbon working electrode, a platinum wire counter electrode, and an SCE reference electrode in contact with the cell through a CH_2Cl_2/^{t}-$Bu_4N(B(C_6F_5)_4)$ salt bridge (2.0 M). The glassy carbon electrode was activated according to the methods of Thorp and co-workers.[58] Scan rates utilized for these two complexes ranged between 0.5 and 2.5 V s^{-1}. For $\mathbf{1^{Me_2N}}$, a 10 μm diameter platinum ultramicroelectrode was used as the working electrode. The concentrations of electrolyte and copper complex were kept the same as those listed above.

Reduction potentials were also obtained by spectroeletrochemical "titrations" using ferrocene derivatives (ferrocene for $\mathbf{1^H}$, ethylferrocene for $\mathbf{1^{MeO}}$, and dimethylferrocene for $\mathbf{1^{Me_2N}}$). In a typical experiment, a solution of $\sim 5 \times 10^{-5}$ M $\mathbf{1^R}$ in CH_2Cl_2 was cooled to −78 °C. A solution of the ferrocene derivative was then added to the copper solution and mixed gently with argon for ∼5 s. Reduction of the Cu_2O_2 complex was noted by the decrease in the charge-transfer band of $\mathbf{1^R}$

Table 2. Comparison of Geometric Parameters for Structures Discussed Here

distances and angles	$\mathbf{2^{MeO}}$	$\mathbf{2^{Me_2N}}$	$\mathbf{2^H}$	$\mathbf{1^H}$ [a]
Cu−O	1.945(2)	1.951(3)	1.958(3)	1.905(5)
Cu−O	1.946(3)	1.944(3)	1.948(3)	1.922(6)
$Cu-N_{amine/PY}$ (axial)	2.277(2) (NR_3)	2.302(2) (NR_3)	2.234(4) (py)	2.177(6) (py)
$Cu-N_{PY/amine}$(eq)	2.011(3) (py)	2.011(3) (py)	2.075(4) (NR_3)	2.027(6) (NR_3)
$Cu-N_{PY}$ (eq)	2.000(2)	2.004(4)	2.005(4)	1.989(6)
Cu/N_2O_2 plane[b]	0.279	0.250	0.215	
Cu···Cu	3.057(1)	3.037(1)	3.012(1)	3.445(2)
$N_{eq/PY}-Cu-N_{ax}$	93.4(1)	90.6(1)	96.7(1)	97.9(3)
$N_{eq/PY(amine)}-Cu-N_{ax}$	96.0(1)	96.2(1)	96.7(1)	103.1(3)
$N_{eq/PY(amine)}-Cu-N_{eq}$	95.1(1)	94.1(1)	94.3(2)	98.2(3)
τ[c]	0.07	0.09	0.04	0.06

[a] Intermediate structure as a mixture of peroxo and bis-μ-oxo isomers.[67] [b] Distance (Å) of Cu(II) out of the basal plane. [c] With $(a - b)/60$ (a = largest interatomic angle including Cu; b = second largest such angle); square pyramid, $\tau = 0.0$; trigonal bipyramid, $\tau = 1.0$.[79]

centered around 355 nm (ϵ = 16 000−23 000 M^{-1} cm^{-1}). The end point was determined by noting no further change in the electronic absorption spectrum at 355 nm upon further addition of ferrocene or derivative.

EPR Experiments. 1^R in 0.25 mL of a 1:1 mixture of CH_2Cl_2/toluene (2×10^{-4} M) was prepared in an EPR tube at −78 °C in a dry ice/acetone bath. A cold solution of 0.05 mL of CH_2Cl_2 solution of substrate (0.1 equiv of decamethylferrocene of TEMPO-H) was then injected into the EPR tube, and then the tube was quickly immersed in liquid nitrogen. EPR spectra were then recorded at 65 K as frozen glasses. In the case of TEMPO-H, we determined the yield of TEMPO• formed in the reaction by integrating the EPR spectra and comparing this to a standard (2×10^{-4} M) solution of TEMPO•.

X-ray Crystallographic Studies of 2^{MeO} and 2^{Me_2N}. Both 2^{MeO} and 2^{Me_2N} compounds were prepared by the oxidative decomposition of 1^{MeO} and 1^{Me_2N} in THF and then recrystallized from CH_2Cl_2/pentane. Suitable greenish−blue crystals were mounted with epoxy cement to the tip of a glass fiber. Intensity data were collected at 150(2) K with a Bruker SMART APEX CCD diffractometer with graphite monochromated Mo Kα radiation (λ = 0.71073 Å). An absorption correction was done using the SADABS program (Sheldrick, G. M. SADABS (2.01), Bruker/Siemens Area Detector Absorption Correction program, Bruker AXS, Madison, WI, 1998). The structure was solved by direct methods, completed by difference Fourier syntheses, and refined by full-matrix least-squares refinement procedures based on F^2. All non-hydrogen atoms were refined with anisotropic thermal parameters and assigned to idealized geometric positions using a rigid group model. All software and sources of the scattering factors are contained in the SHELXTL (5.1) program library (G. Sheldrick, Siemens XRD, Madison, WI). Relevant crystallographic information and the main details of the diffraction experiment and refinement of the crystal structure are provided in Table 2, while the full X-ray structural reports (in CIF format) may be found in the Supporting Information.

Results

This study is aimed at better understanding the fundamental mechanism of PCET oxidation reactions mediated by peroxo complexes, $[\{Cu^{II}(MePY2)^R\}_2(O_2^{2-})]^{2+}$ ($\mathbf{1^R}$). We first present our survey of the scope of PCET reactions that can or cannot be facilitated by $\mathbf{1^R}$. Next, we briefly discuss relevant thermodynamic properties of $\mathbf{1^R}$ pertaining to such reactions, that is, one-electron reduction potentials, and how oxo/peroxo protonation influences ET reactions. We then present kinetic and reactivity studies aimed at better understanding the mechanism of $\mathbf{1^R}$ substrate oxidation reactions.

Oxidation Reaction Facilitated by $[\{Cu^{II}(MePY2)^R\}_2(O_2)]^{2+}$ ($\mathbf{1^R}$). Cu−dioxygen adducts $[\{Cu^{II}(MePY2)^R\}_2(O_2)]^{2+}$ ($\mathbf{1^R}$) are capable of performing several oxidation reactions, including O atom transfers (PPh_3 to $O{=}PPh_3$)[59] and formal hydrogen atom (H•) abstraction reactions (tetrahydrofuran (THF) to 2-hydroxytetrahydrofuran (THF−OH), alcohols to aldehydes and ketones, and dimethylaniline (DMA) to methylaniline (MA) and formaldehyde).[42,44] In the latter case, the resulting copper-containing products are bis-μ-hydroxo complexes, $[\{Cu^{II}(MePY2)^R\}_2(OH)_2]^{2+}$ ($\mathbf{2^R}$), and the organic substrate is either oxidized by (formally) one or two H• or hydroxylated via a "rebound"-type reaction analogous to that of cytochrome P450 chemistry.[42,44]

Scheme 4

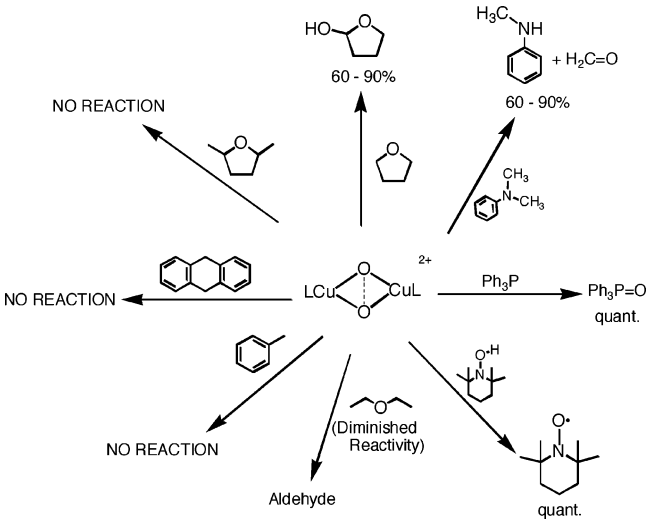

In the present study, we explore other potential substrates that are oxidized by $\mathbf{1^R}$ (Scheme 4) and possess thermodynamic properties similar to those previously examined. Examining thermodynamically similar (i.e., one-electron oxidation potentials and H−X BDEs, X = C or O) but structurally different substrates will also allow us to gain insight into potential substrate structural and/or electronic requirements necessary for $\mathbf{1^R}$ to facilitate substrate oxidation. Toluene oxidation (BDE ∼ 89 kcal mol^{-1})[60] was not facilitated by $\mathbf{1^R}$ despite possessing a C−H bond strength similar to that known for THF (BDE ∼ 92 kcal mol^{-1}).[61] It was also observed that substrates which are structurally similar to THF either showed no reactivity, such as 2,5-dimethyltetrahydrofuran (Me_2THF), or showed diminished (i.e., slower) reactivity, such as diethyl ether.[62] This is despite the fact that these ethers are thermodynamically similar to THF; all have α C−H BDEs of ∼90 kcal mol^{-1}.

Next, we investigated reactions between $\mathbf{1^R}$ and substrates with significantly *weaker* X−H bonds (where X = C or O). TEMPO-H (2,2,6,6-tetramethylpiperidin-1-ol), which has an O−H BDE of ∼70 kcal mol^{-1},[63] reacts with $\mathbf{1^R}$ exceptionally fast and quantitatively at −80 °C, affording $\mathbf{2^R}$ and 2 equiv of TEMPO• as the only organic product; see further discussion below.[64] Both EPR spin integration (vide infra) and UV−vis titrations demonstrate that 2 equiv of TEMPO-H gives 2 equiv of TEMPO• and 1 equiv of $\mathbf{2^R}$.

Previously, we had stated that $\mathbf{1^R}$ would react with 9,10-dihydroanthracene (DHA, which has a C−H BDE of ∼78 kcal mol^{-1}) at low temperatures.[42,65] Reinvestigation of DHA oxidation now reveals that, in fact, it will *not* undergo a redox reaction with $\mathbf{1^R}$ under the conditions investigated (−80 °C in CH_2Cl_2).

(56) Wilkins, R. G. *Kinetics and Mechanism of Reactions of Transition Metal Complexes*, 2nd ed.; VCH: New York, 1991.
(57) Furniss, B. S.; Hannaford, A. J.; Smith, P. W. G.; Tatchell, A. R. *Vogel's Textbook of Practical Organic Chemistry*, 5th ed.; Pearson Education Ltd.: Essex, England, 1989.
(58) Thorp, H. H.; Sarneski, J. E.; Brudvig, G. W.; Crabtree, R. H. *J. Am. Chem. Soc.* **1989**, *111*, 9249−9250.
(59) Obias, H. V.; Lin, Y.; Murthy, N. N.; Pidcock, E.; Solomon, E. I.; Ralle, M.; Blackburn, N. J.; Neuhold, Y.-M.; Zuberbühler, A. D.; Karlin, K. D. *J. Am. Chem. Soc.* **1998**, *120*, 12960−12961.
(60) Berkowitz, J.; Ellison, G. B.; Gutman, D. *J. Phys. Chem.* **1994**, *98*, 2744−2765.
(61) Laarhoven, L. J. J.; Mulder, P. *J. Phys. Chem. B* **1997**, *101*, 73−77.
(62) Due to the low yields and low molecular weights of products in diethyl ether oxidations, we were only able to confirm that an aldehyde was produced. This suggests an oxidative O-dealkylation through a rebound-like process.
(63) Bordwell, F. G.; Liu, W.-Z. *J. Am. Chem. Soc.* **1996**, *118*, 10819−10823.
(64) The reaction is too fast for us to monitor by stopped-flow methods (i.e., TEMPO-H oxidation is faster than dioxygen adduct formation), that is, the overall reaction observed is $[Cu^{I}(MePY2)]^+ \rightarrow \mathbf{2^R}$).
(65) Bordwell, F. G.; Cheng, J.; Ji, G. Z.; Satish, A. V.; Zhang, X. *J. Am. Chem. Soc.* **1991**, *113*, 9790−9795.

Scheme 5

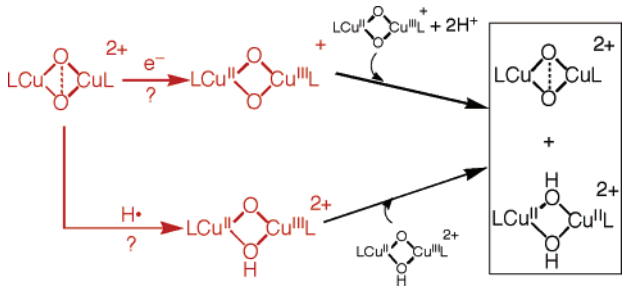

In the earlier study, organic product reaction yields were analyzed by GC after 24 h from the start of the reaction. Doing so involves a workup where the reaction mixture is warmed and then passed through a plug of alumina prior to GC/MS analysis to remove all copper-containing products. It is during this warmup that DHA oxidation appears to occur. Dichloromethane solutions of $\mathbf{1^R}$ kept at −80 °C for 7 days show no reactivity toward DHA. Instead, UV−vis monitoring shows that $\mathbf{1^R}$ "autodecomposes" to $\mathbf{2^R}$ through an unidentified oxidation pathway at a rate identical to that when no substrate is present ($k < 10^{-6}$ s^{-1}). Furthermore, no anthracene product is observed, as noted by both GC and UV−vis spectroscopies.

Thus, it appears that for $\mathbf{1^R}$ substrate oxidations, thermodynamic considerations (i.e., X−H BDEs) cannot adequately predict which substrates will react. Scheme 4 shows a summary of the reactivity of $\mathbf{1^R}$ that we investigated for the current and previous studies, excluding the reactivity probe studies described below.

Thermodynamic Properties of $\mathbf{1^R}$. We next sought to determine the oxidizing abilities of $[\{Cu^{II}(MePY2)^R\}_2(O_2)]^{2+}$ to determine if proton-*un*coupled reactions (i.e., single-electron oxidation (SET)) by $\mathbf{1^R}$ are thermodynamically uphill by obtaining *approximate* redox potentials. SET oxidations effected by $\mathbf{1^R}$ might, in principle, produce a one-electron-reduced mixed-valence dicopper $[Cu^{II}Cu^{III}(O)_2]^+$ species (see Scheme 5).

Cyclic voltammetry studies of $[\{Cu^{II}(MePY2)^R(O_2)]^{2+}$ ($\mathbf{1^R}$) were carried out in CH_2Cl_2 at −78 °C. Complexes $\mathbf{1^R}$ are reasonably stable toward the supporting electrolyte, 0.1 M $Bu_4N(B(C_6F_5)_4)$. The latter has been shown to improve the quality of electrochemical data recorded in solvent with low dielectric constants at low temperatures.[53] Reasonably "clean" reductions that can best be described as quasi-reversible are observed for both $\mathbf{1^H}$ and $\mathbf{1^{MeO}}$ (Figure 1). We can, therefore, estimate reduction potentials (E_{red}), ∼550 mV for $\mathbf{1^H}$ and ∼400 mV for $\mathbf{1^{MeO}}$, based on the apparent midpoints of the reduction waves. In contrast, $\mathbf{1^{Me_2N}}$ does not yield readily interpretable electrochemical data by CV, even with the use of a platinum ultramicroelectrode at a scan velocity of 51 V s^{-1}. This is presumably due to $\mathbf{1^{Me_2N}}$s extreme instability toward reducing conditions (see Supporting Information for a representative CV of $\mathbf{1^{Me_2N}}$).

To put an upper limit on the SET oxidizing ability of $\mathbf{1^R}$, we decided to expose solutions of $\mathbf{1^R}$ to ferrocene derivatives that are progressively harder to oxidize. Here, we can monitor the reduction of $\mathbf{1^R}$, and hence the oxidation of the ferrocene derivative, by observing the quenching of the peroxo → Cu^{II} ligand-to-metal charge transfer (LMCT) at ∼355 nm (360 nm for $\mathbf{1^{Me_2N}}$) by UV−vis spectroscopy upon the addition of the appropriate ferrocene derivative (see Supporting Information Figure S2). It was determined that addition of a slight excess

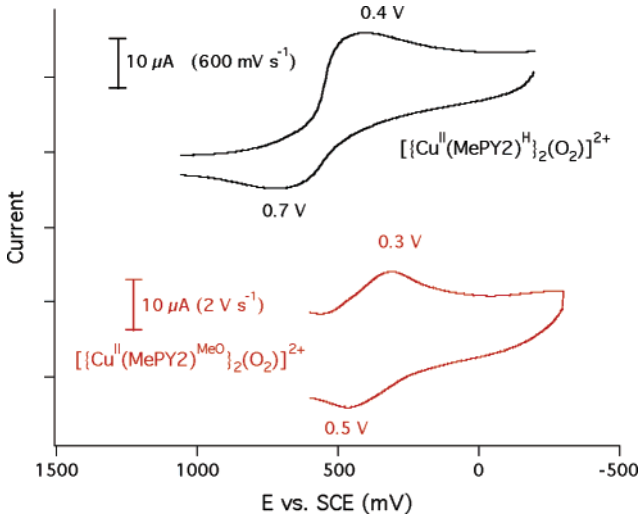

Figure 1. Cyclic voltammograms of $\mathbf{1^H}$ (black) and $\mathbf{1^{MeO}}$ (red) recorded at −78 °C in CH_2Cl_2 with $Bu_4N(B(C_6F_5)_4)$ as the supporting electrolyte.

of ferrocene ($E_{1/2}$ = 560 mV in CH_2Cl_2) to $\mathbf{1^H}$ resulted in the complete quenching of its LMCT band. However, excess ferrocene was incapable of readily reducing either $\mathbf{1^{MeO}}$ or $\mathbf{1^{Me_2N}}$. On the other hand, $\mathbf{1^{MeO}}$ is readily reduced by excess ethylferrocene ($E_{1/2}$ = 380 mV versus SCE in CH_2Cl_2), while $\mathbf{1^{Me_2N}}$ required the substrate, dimethylferrocene ($E_{1/2}$ = 230 mV versus SCE in CH_2Cl_2), for its reduction. On the basis of these experiments/evidence, it appears that the complex with the least electron-donating 4-pyridyl substituent ($\mathbf{1^H}$) is the most oxidizing, while the complex with the most electron-donating substituent ($\mathbf{1^{Me_2N}}$) is the least powerful oxidant; not surprisingly, the more electron-donating ligand can better support and stabilize the higher oxidation state, making it less reactive.

Dichloromethane solutions of $\mathbf{1^R}$ are stable at −80 °C in the presence of the weak reductant, $[Fe^{II}(phen)_2(NO_2\text{-phen})](ClO_4)_2$ ($E_{1/2}$ = 1.3 V versus SCE in CH_2Cl_2). However, the addition of a slight excess of $NH_4(B(C_6F_5)_4)$ (pK_a = 16.5 in MeCN at 25 °C)[66] as an acid/proton source leads to the rapid decay of the band at 355 nm (360 nm for $\mathbf{1^{Me_2N}}$), demonstrating the reduction of the Cu_2−dioxygen adducts. The resulting products are the corresponding two-electron/two-proton-reduced (relative to $\mathbf{1^R}$) bis-μ-hydroxo complexes, $[\{Cu^{II}(MePY2)^R\}_2(OH)_2]^{2+}$ ($\mathbf{2^R}$) and $[Fe^{III}(phen)_2(NO_2\text{-phen})_2]^{3+}$ (as assessed by UV−vis spectroscopy). When acetic acid is instead used as a proton source (pK_a = 22.3 in MeCN at 25 °C)[66] under otherwise identical conditions, no immediate observable reaction takes place. The results, discussed further below, suggest coupling protonation with a weak reductant can, in fact, lead to PCET-type reduction of the peroxo complexes $\mathbf{1^R}$.

Oxidation Reactions Probed by EPR. We next sought to determine if a mixed-valence dicopper μ-oxo μ-hydroxo species, $[Cu_2(O)(OH)]^{2+}$, could be readily produced from $[\{Cu^{II}(MePY2)^R\text{-}(O_2)]^{2+}$ ($\mathbf{1^R}$) by using less than 1 equiv of an easily oxidized H$^\bullet$ or e$^-$ donor (see Scheme 5). Such species are likely to be "initial" intermediates in hydrogen atom abstraction oxidation reactions;[31,44,67,68] however, their instability may preclude observation. Reactions between H$^\bullet$ or e$^-$ donors and $\mathbf{1^R}$ were performed in an EPR tube at −78 °C, and then the resulting

(66) Izutsu, K. *Acid−Base Dissociation Constants in Dipolar Aprotic Solvents*; Blackwell Scientific Publications: Oxford, U.K., 1990; Chemical Data Series, No. 35.

solutions were quickly frozen in a liquid nitrogen bath. These frozen glasses were subjected to analysis by EPR spectroscopy. To test for single versus double ET to $\mathbf{1^R}$, $^1/_{10}$ of an equivalent of decamethylferrocene was added per copper, which reacted quantitatively with $\mathbf{1^R}$ at −78 °C (UV−vis monitoring). This resulted in the formation of an EPR silent solution (at 65 K), consistent with the conversion of all decamethylferrocene into decamethylferrocenium ion, which has a ground spin state of $^3/_2$ and would not be observable at this high temperature. Also, this suggests that a $Cu^{II}Cu^{III}$ mixed-valence complex was not stable under these conditions, and that the copper complex generated was fully reduced. If a mixed-valence compound was formed, it should have an easy-to-observe distinctive EPR spectrum, resulting from electron delocalization over the two copper ($I = {}^3/_2$) centers. Similarly, $^1/_{10}$ of an equivalent of TEMPO-H results in the complete formation of TEMPO$^\bullet$ (as assessed by EPR spin integration), but no signal that could be attributed to a Cu^{II}/Cu^{III} dimer is seen. This also suggests that molecules of $[\{Cu^{II}(MePY2)^R(O_2)]^{2+}$ ($\mathbf{1^R}$) are reduced by two hydrogen atoms, independent of the amount of TEMPO-H reductant added (i.e., less than stoichiometric amounts).

To summarize, we could not generate a Cu^{II}/Cu^{III} binuclear complex by the addition of a substoichiometric amount of a reductant or a H-atom donor. Furthermore, these data seem to suggest that 2 equiv of $FeCp_2^R$ and TEMPO-H is consumed per Cu−peroxo binuclear complex, $[\{Cu^{II}(MePY2)^R(O_2)]^{2+}$ ($\mathbf{1^R}$), possibly through a disproportionation reaction (Scheme 5; see Discussion).

Oxidation of THF by $\mathbf{1^{Me_2N}}$. It was previously noted that THF solutions of $[\{Cu^{II}(MePY2)^R(O_2)]^{2+}$ ($\mathbf{1^R}$) are unstable, with $\mathbf{1^R}$ readily converted into $[\{Cu^{II}(MePY2)^R\}_2(OH)_2]^{2+}$ ($\mathbf{2^R}$) over the course of several minutes to hours (depending on R).[69,70] A further study using dichloromethane solutions of THF demonstrated that this substrate is, in fact, being oxidized by $\mathbf{1^R}$ to THF−OH; the oxygen atom incorporated into the THF−OH product is derived from the peroxo moiety of $\mathbf{1^R}$.[42] Here, we present new data and insights for THF oxidation by $\mathbf{1^{Me_2N}}$. Difficulties were seen to arise for THF oxidation by $\mathbf{1^H}$ and $\mathbf{1^{MeO}}$, as kinetics of THF oxidation are complicated by the presence of the MeCN ligand found in the starting material complexes, $[Cu^I(MePY2)^R(MeCN)]^+$ (R = H or MeO).[42] As seen previously, small variable amounts of MeCN complicate O_2 complex formation,[42b] and here, differing quantities of MeCN dramatically slow THF oxidation by $\mathbf{1^H}$ and $\mathbf{1^{MeO}}$. However, the variations are not predictable, quite possibly due to variable contamination of $[Cu^I(MePY2)^R(MeCN)]^+$ by $[Cu^I(MePY2)^R]^+$, the Cu^I complex with a "lost" acetonitrile ligand. The MeCN ligand is not ever present in $[Cu^I(MePY2)^{Me_2N}]^+$,[42] which is a pure three-coordinate complex. It should be noted that the additional MeCN derived from the Cu^I starting material does not appear to influence the kinetics of $\mathbf{1^H}$ or $\mathbf{1^{MeO}}$ oxidation of dimethylaniline (DMA) (vide infra).

Dichloromethane solutions of $\mathbf{1^{Me_2N}}$ readily and rapidly oxidize THF over the temperature range of −90 to −70 °C (see Supporting Information). Oxidation rate constants were determined by both stopped-flow and benchtop UV−vis kinetic techniques, each of which gave data consistent with one another. No UV−vis detectable intermediates were observed in the oxidation of THF by $\mathbf{1^{Me_2N}}$; only the clean conversion of $\mathbf{1^{Me_2N}}$ to $\mathbf{2^{Me_2N}}$ is noted. Under pseudo-first-order conditions ([THF] = 0.1−2.0 M), plots of k_{obs} versus [THF] demonstrated second-order behavior (first order in THF, first order in $\mathbf{1^{Me_2N}}$), with rate constants ranging from $8.9(1) \times 10^{-3}$ M^{-1} s^{-1} at −90 °C to $2.9(1) \times 10^{-2}$ M^{-1} s^{-1} at −70 °C. The second-order behavior might seem to suggest a straightforward "outer-sphere"-type oxidation mechanism in the conversion of THF to THF−OH by $\mathbf{1^{Me_2N}}$.[71] However, an Eyring analysis demonstrates that THF oxidation by $\mathbf{1^{Me_2N}}$ proceeds with a very low activation enthalpy of 3.7(1) kcal mol^{-1}, which strongly implicates the presence of a rapid but left-lying pre-equilibrium which occurs prior to the THF oxidation step, possibly that involving THF coordination.[72] (Such a pre-equilibrium involving substrate binding is clearly evident in the oxidation of DMA by $\mathbf{1^R}$, vide infra.) Thus, the THF oxidation mechanism is perhaps better described as "inner-sphere oxidation" because of the likely substrate binding step.

Reactions of $\mathbf{1^R}$ with *N,N′*-Dimethylaniline (DMA). As previously described,[44] −85 to −65 °C dichloromethane solutions of $\mathbf{1^R}$ rapidly oxidize DMA to formaldehyde and methylamine (MA) within several minutes (see Scheme 4). Here, our further studies show that observed first-order rate constants (k_{obs}) plotted against substrate concentration ([DMA] ranging between 0.8 and 30 mM) exhibit Michaelis−Menten-type saturation kinetics at higher DMA concentrations (Figure 2). Fitting these data to eq 1 (vide supra) allowed us to extract both an equilibrium constant (K_{eq}) for DMA binding and subsequent first-order oxidation rate constants (k_{ox}) for DMA oxidation (Scheme 6). The $\mathbf{1^R}$ series exhibit fairly weak binding of DMA, as may be expected, with K_{eq} varying between approximately 850 and 10 M^{-1} over the temperature range of −85 to −65 °C (see Supporting Information). A van't Hoff analysis provides estimates of the thermodynamic parameters; DMA binding is enthalpically favored ($\Delta H° > 10$ kcal mol^{-1}), while it is strongly disfavored entropically, as would be expected ($\Delta S° < -40$ cal mol^{-1} K^{-1}; see Supporting Information).[73] DMA binding to $\mathbf{1^{MeO}}$ ($K_{eq}^{-75\,C} = 140(30)$ M^{-1}) appears to be stronger than that observed for $\mathbf{1^H}$ ($K_{eq}^{-75\,C} = 27(11)$ M^{-1}), while DMA binding to $\mathbf{1^{Me_2N}}$ ($K_{eq}^{-75\,C} = 105(45)$ M^{-1}) is intermediate (Supporting Information).

Oxidation rates at low temperatures (≤−80 °C) appear to follow trends related to the electron-donating abilities of the 4-pyridyl ligand substituent. Concerning these DMA reactions, the more electron-rich metal center in $\mathbf{1^{Me_2N}}$ affords reaction rate constants ($k_{ox} = 3.4(1) \times 10^{-1}$ s^{-1} at −85 °C) nearly an order of magnitude larger than that for $\mathbf{1^{MeO}}$ ($k_{ox} = 1.1(1) \times 10^{-2}$ s^{-1} at −85 °C), and nearly 2 orders of magnitude faster than that of $\mathbf{1^H}$ ($k_{ox} = 5.5(1) \times 10^{-3}$ s^{-1} at −85 °C). These findings may seem to be unexpected, with the strongest oxidant,

(67) Pidcock, E.; DeBeer, S.; Obias, H. V.; Hedman, B.; Hodgson, K. O.; Karlin, K. D.; Solomon, E. I. *J. Am. Chem. Soc.* **1999**, *121*, 1870−1878.
(68) Chan, S. I.; Chen, K. H. C.; Yu, S. S. F.; Chen, C. L.; Kuo, S. S. J. *Biochemistry* **2004**, *43*, 4421−4430.
(69) Zhang, C. X. Johns Hopkins University, 2001.
(70) Obias, H. V. Johns Hopkins University, 1998.

(71) An initial rate-limiting oxidation event combined with the fact that the transferred oxygen atom is derived from the peroxo moiety suggests that THF oxidation to 2-hydroxytetrahydrofuran occurs through a rebound-type mechanism similar to that of cytochrome P450 chemistry.[42]

(72) (a) Karlin, K. D.; Kaderli, S.; Zuberbühler, A. D. *Acc. Chem. Res.* **1997**, *30*, 139−147. (b) Zhang, C. X.; Kaderli, S.; Costas, M.; Kim, E.-i.; Neuhold, Y.-M.; Karlin, K. D.; Zuberbühler, A. D. *Inorg. Chem.* **2003**, *42*, 1807−1824.

(73) Weak binding at higher temperatures adds a great deal of uncertainty in reported K_{eq} values, which leads to uncertainty in the calculated $\Delta S°$ term. See further details in the Discussion.

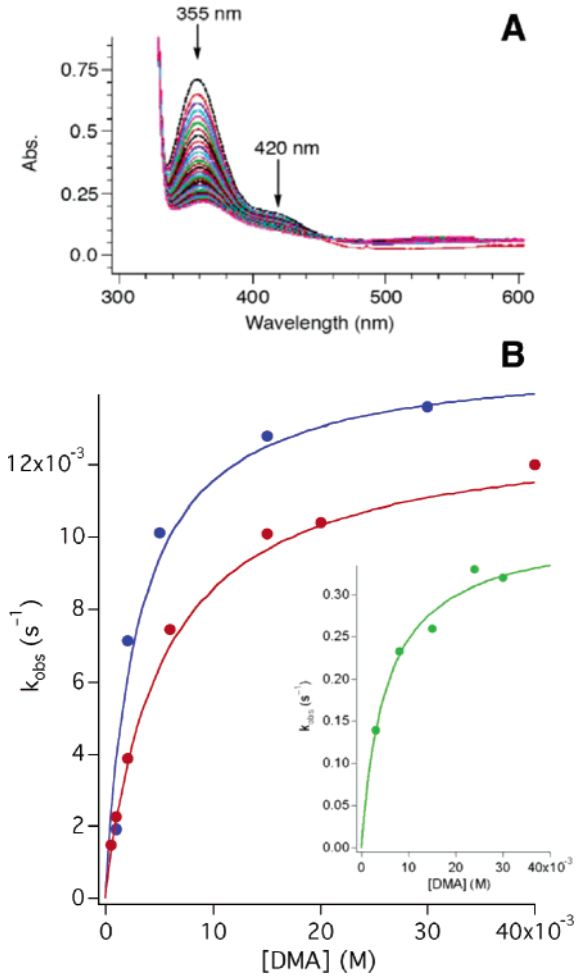

Figure 2. (A) DMA oxidation reaction monitored by the decay of the λ_{max} = 355 nm absorption due to peroxo complex $\mathbf{1^H}$ in CH_2Cl_2 at −80 °C {[DMA] = 6.0 mM; time = 3000 s; time interval = 30 s}. (B) Observed first-order rate constants (k_{obs}) as a function of DMA concentration for $\mathbf{1^H}$ (red) and $\mathbf{1^{MeO}}$ (blue) oxidation of DMA at −80 °C in CH_2Cl_2. The experimental data are shown as solid circles, and the best fit is displayed as the solid line. The inset plots k_{obs} for DMA oxidation by $\mathbf{1^{Me_2N}}$ (green) versus DMA concentration at −80 °C in CH_2Cl_2. Trend lines are based on fits to the data according to $k_{obs} = k_{ox}[DMA]/(K_{eq} + [DMA])$.[74]

Scheme 6

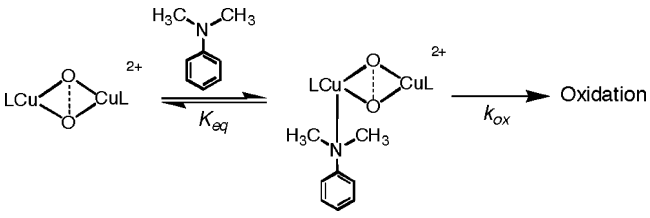

$\mathbf{1^H}$, affording the *slowest* oxidation rates, and this subject is further discussed below. This trend appears to hold at higher temperature. However, due to the weak binding of DMA at higher temperatures (Supporting Information Table S2), extraction of accurate oxidation rate constants is difficult, and further comment/conclusions reached concerning the rate data obtained would be unwarranted. It should be pointed out that the presence of additional "free" O_2 in the reaction mixtures (i.e., not purging the reactions with argon) did not significantly change the calculated DMA rates or binding constants to $\mathbf{1^R}$.

Reactions With Mechanistic Probes: *N*-Cyclopropyl-*N*-methylaniline (CMA). CMA was used as a probe to investigate

Scheme 7

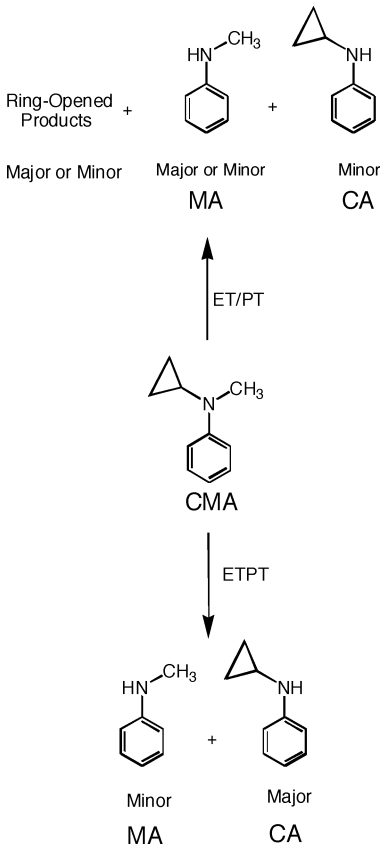

whether these complexes support concerted or consecutive proton-coupled reactions (ETPT versus ET/PT).[34] If CMA is oxidized by $\mathbf{1^R}$ through an ETPT pathway, then *N*-methyl dealkylation should be the prevalent oxidation pathway (producing *N*-cyclopropylaniline (CA)), with *N*-cyclopropyl dealkylation being the minor oxidation pathway (producing MA).[75] However, under ET/PT conditions, CA is a minor (<5%) product;[76] furthermore, this pathway will also result in a cyclopropyl ring opening, which can then produce a wide variety of observable organic products.[45,47,76] This is summarized in Scheme 7.

Actual reactions between $\mathbf{1^R}$ and 10 molar equiv of CMA are relatively fast, going to completion within a 24 h period. The mixture produced when CMA is oxidized by $\mathbf{1^{MeO}}$ and $\mathbf{1^H}$ is rich in products, including a compound we tentatively assign as *ortho*-(propan-3-al)-*N*-methylaniline (PMA)[77] (20−30%) based on GC/MS (*m*/*z* = 163.1) analysis and mechanistic considerations (see Discussion). MA (50−60%) and a small amount of CA (<6%) (Scheme 7) are also observed in the reaction mixture. These yields assume that one substrate CMA is oxidized per dicopper $\mathbf{1^R}$ oxidant. There is at least one other product obtained in the oxidation of CMA by $\mathbf{1^H}$ and $\mathbf{1^{MeO}}$, as assessed by GC/MS, which has eluded identification (see Supporting Information).

In contrast, there are relatively few oxidation products observed by GC/MS for CMA oxidation by $\mathbf{1^{Me_2N}}$, with MA

(74) Ambundo, E. A.; Friesner, R. A.; Lippard, S. J. *J. Am. Chem. Soc.* **2002**, *124*, 8770−8771.
(75) Shaffer, C. L.; Harriman, S.; Koen, Y. M.; Hanzlik, R. P. *J. Am. Chem. Soc.* **2002**, *124*, 8268−8274.
(76) Bhakta, M. N.; Wimalasena, K. *J. Am. Chem. Soc.* **2002**, *124*, 1844−1845.
(77) Attempts were made to obtain a pure standard of PMA. These attempts all yielded impure material which quickly decomposed into a brown polymeric substance, presumably due to inter- and intramolecular iminium formation between the aldehyde and methylamine moiety.

Scheme 8

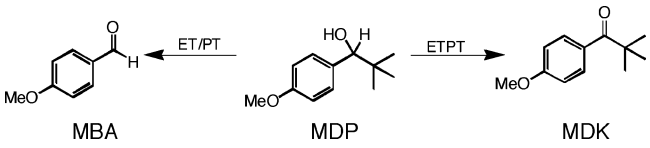

and CA produced in relatively low yields (~2% each). It should be noted that the oxidation product seen with $\mathbf{1^H}$ and $\mathbf{1^{MeO}}$, which we assigned to PMA, is not produced in this reaction. A nonvolatile compound was obtained following column chromatography of the reaction mixture, which was identified (by ^{1}H NMR spectroscopy; see Supporting Information) as the *N*-methylquinolinium cation (MQ^+), presumed to be isolated with the $B(C_6F_5)_4^-$ counteranion since (i) the MQ^+ salt is *highly* soluble in organic solvents, (ii) readily moved down a silica column, and (iii) showed no ^{1}H-NMR signal arising from the counteranion. Due to the cationic nature of MQ^+, we have been unable to determine exact yields; however, this *is* the major oxidation product present in ~50% (or possibly 100%; see Discussion) yield, as indicated by gravimetric analysis. To overview, these results (summarized in Table 1, see Experimental Section) strongly suggest that $\mathbf{1^R}$ oxidizes CMA through an ET/PT pathway (also see Scheme 7 and Discussion below).

MDP Oxidation. The oxidation of (*p*-methoxyphenyl)-2,2-dimethylpropanol (MDP) by $\mathbf{1^R}$ in CH_2Cl_2 at −80 °C was also investigated. Under ETPT conditions, MDP loses two hydrogen atoms (formally), resulting in the formation of (*p*-methoxyphenyl)-2,2-dimethylpropanone (MDK), while an ET/PT pathway results in an unstable radical cation, which undergoes an $\alpha-\beta$ C−C bond cleavage and leads to the formation of *p*-methoxybenzaldehyde (MBA) (see Scheme 8).[46]

Reaction times were significantly longer for MDP than for CMA oxidations, requiring several days for the reaction to go to completion, as followed by the disappearance of $\mathbf{1^R}$ and the appearance of $\mathbf{2^R}$. Conversion of the peroxo complexes $\mathbf{1^R}$ to the bis-μ-hydroxo complexes $\mathbf{2^R}$ is accelerated in the presence of MDP compared to "autodecomposition" (i.e., with no substrate present); however, the latter pathways must compete since the overall yields of organic product were significantly lower when compared to those of CMA oxidations; yields ranged from 40 to 60% depending on the metal complex (Table 2). Curiously, the complex with the most electron-donating 4-pyridyl substituent ($\mathbf{1^{Me_2N}}$) not only afforded the highest yield of oxidized product but also approached completion the fastest. As with CMA oxidation (vide supra), this may be unexpected considering it is the weakest (one-electron) oxidant of the $\mathbf{1^R}$ series. MDP oxidation by $\mathbf{1^{MeO}}$ and $\mathbf{1^{Me_2N}}$ produced only MDK as the oxidation product, suggesting an ETPT mechanistic pathway (Scheme 8). For MDP oxidation by $\mathbf{1^H}$, the major product was MBA, with MDK observed as a minor product, suggesting that *both* ETPT and ET/PT pathways may be operable.[78]

X-ray Crystallographic Studies of $\mathbf{2^{MeO}}$ and $\mathbf{2^{Me_2N}}$. Refinement parameters for $[\{Cu^{II}(MePY2)^{MeO}\}_2(OH)_2]^{2+}$ ($\mathbf{2^{MeO}}$) and $[\{Cu^{II}(MePY2)^{Me_2N}\}_2(OH)_2]^{2+}$ ($\mathbf{2^{Me_2N}}$) are given in the Supporting Information (Table S1), and selected structural metric parameters are displayed here in Table 2. Figures 3 and 4 provide representations of these Cu^{II}_2−bis-μ-hydroxo complexes, while Figures 5 and 6 show the previously described structures of $\mathbf{2^H}$ and $\mathbf{1^H}$, respectively (a mixture; see discussion below).[59,67,70] Structural comparisons (see also Table 2) show that the μ-$(OH^-)_2$ (all $\mathbf{2^R}$) and μ-η^2:η^2-peroxo or μ-$(O^{2-})_2$ (ligand)−Cu groups (in $\mathbf{1^H}$) lie in equatorial positions. For $\mathbf{2^H}$ and $\mathbf{1^H}$, the coordination of the tridentate pyridyl ligand is nearly identical in terms of wrapping around the copper ion. In both cases, one pyridyl arm is bound axially; the alkylamine nitrogen is bound equatorially, and the other pyridyl arm is bound in a pseudoequatorial position. By contrast, the crystal structures of $\mathbf{2^{MeO}}$ and $\mathbf{2^{Me_2N}}$ reveal a completely different ligand coordination geometry, which results in near C_{2h} symmetry for the metal complex. In these cases, *both* pyridyl arms are bound in

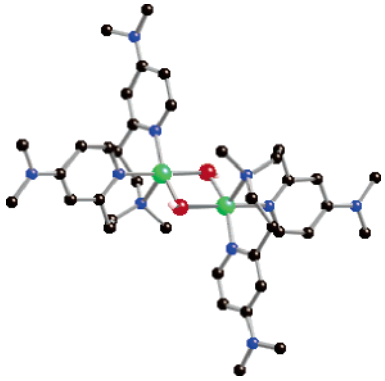

Figure 3. Representation of the cationic portion of $\mathbf{2^{Me_2N}}$, generated from the compound cif file using CrystalMaker 6.3 (CrystalMaker, Ltd., Yarnton, Oxfordshire, U.K.). Hydrogen atoms (except those bound to the hydroxo core) have been removed for clarity.

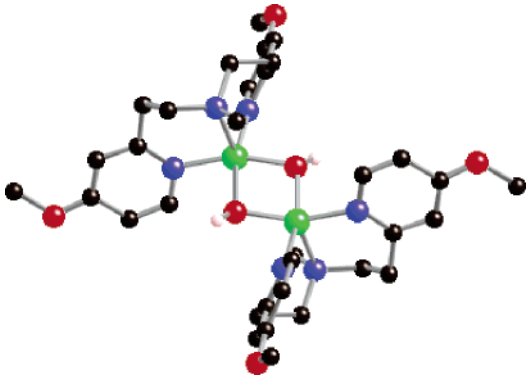

Figure 4. Representation of the cationic portion of $\mathbf{2^{MeO}}$, generated from the compound cif file using CrystalMaker 6.3 (CrystalMaker, Ltd., Yarnton, Oxfordshire, U.K.). Hydrogen atoms (except those bound to the hydroxo core) have been removed for clarity.

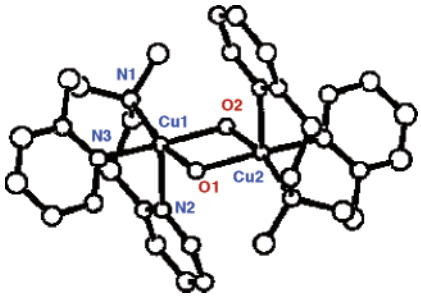

Figure 5. Representation (ChemDraw 3D) of the previously reported crystal structure of $\mathbf{2^H}$.[53] Note the different way in which the pyridylalkylamine tridentate $(MePY2)^H$ ligand (see Introduction) is wrapped about the copper ions, contrasting with that observed for $\mathbf{2^{MeO}}$ and $\mathbf{2^{Me_2N}}$.

(78) No change in product distributions is noted if the reaction temperature is increased to −60 °C, which is the highest temperature at which these complexes will cleanly oxidize substrates.

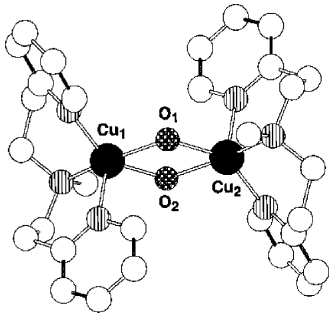

Figure 6. Representation (ChemDraw 3D) of the previously described crystal structure of $\mathbf{1^H}$, the mixed species peroxo/bis-μ-oxo complex with the $(MePY2)^H$ ligand.[63,68] Note the similarities between the crystal structure of this bis(μ-OH−)dicopper(II) complex $\mathbf{2^H}$ (Figure 5) but the different way in which the pyridylalkylamine tridentate ligand is wrapped about the metal compared to that in $\mathbf{2^{MeO}}$ and $\mathbf{2^{Me_2N}}$ (Figures 3 and 4).

Scheme 9. $[\{(MePY2)^RCu^{II}\}_2(OH)_2]^{2+}$ ($\mathbf{2^R}$) Complex Structures

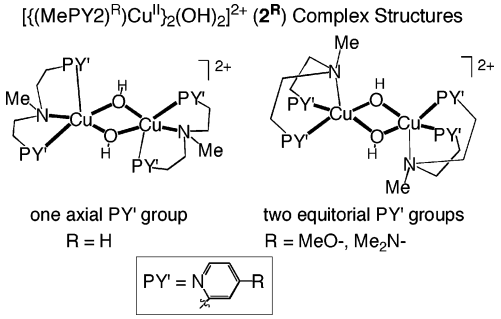

equatorial positions, while the alkylamine−nitrogen is weakly bound axially, Cu−N = 2.27−2.30 Å (Table 2 and Scheme 9). These results indicate that stronger donor substituted pyridines (i.e., MeO− or Me_2N−) prefer to bind equatorially within the square-based pyramidal μ-hydroxo complexes, $\mathbf{2^{MeO}}$ and $\mathbf{2^{Me_2N}}$. Thus, we suggest that in structurally similar[8] μ-peroxodicopper(II) (or bis-μ-oxo dicopper(III) isomer forms; see Discussion) complexes, $\mathbf{1^{MeO}}$ and $\mathbf{1^{Me_2N}}$, a similar situation may occur and the coordination (i.e., ligand wrapping) may be different for $\mathbf{1^H}$. Such structural differences or variations may need to be considered to explain certain aspects of the reactivity patterns observed.

Discussion

The major goal of this study was to investigate the initial steps of PCET reactions facilitated by copper−dioxygen adducts, $[\{Cu^{II}(MePY2)^R\}_2(O_2^{2-})]^{2+}$ ($\mathbf{1^R}$). To meet these ends, we utilized several different approaches. First, we investigated the fundamental redox properties of copper−dioxygen adducts $\mathbf{1^R}$, attempting to determine if PCET versus SET reactions can be thermodynamically supported by $\mathbf{1^R}$ in CH_2Cl_2 at −80 °C. We then investigated the oxidation of DMA in some detail to see if substrate coordination likely occurs and then related this back to different PCET reactions that $\mathbf{1^R}$ can (and cannot) support. Finally, we investigated the reaction of $\mathbf{1^R}$ with two different mechanistic probes, CMA and MDP, to determine if these PCET reactions likely involve concerted or consecutive proton-coupled electron-transfer reactions.

Thermodynamics. Copper−dioxygen adducts $\mathbf{1^R}$ all appear to be mild one-electron oxidants with reduction potentials all below ~550 mV versus SCE (−78 °C), with $\mathbf{1^H}$ being the most oxidizing complex and $\mathbf{1^{Me_2N}}$ being the least. This trend may be expected considering the electron-donating abilities of the *para*-substituents, with the least electron-donating ligand ($MePY2^H$) supporting the most strongly oxidizing metal complex. Two methods were utilized to estimate these trends in reduction potentials. One was cyclic voltammetry, which was plagued by problems, including poor signal-to-noise (due to the low temperatures utilized) and the instability of $\mathbf{1^R}$ toward reduction, even on fast time scales. The instability of these complexes toward reducing conditions may explain the nonideal behavior exhibited in the CVs (Figure 1). Nonetheless, we were able to obtain observable reduction waves for $\mathbf{1^H}$ and $\mathbf{1^{MeO}}$ corresponding to 550 and 400 mV versus SCE, respectively.

Complex $\mathbf{1^{Me_2N}}$ yielded CV data that were not interpretable, even at scan velocities exceeding 50 V s^{-1}. Therefore, to supplement these CV studies, reduction reactions between ferrocene derivatives and $\mathbf{1^R}$ were monitored by UV−vis spectroscopy in CH_2Cl_2 at −78 °C. Due to the irreversible nature of the peroxo reduction, we cannot determine exact values for reduction potentials through such methods. However, we can determine the trend in reduction potentials for these complexes and, with the help of the CV data, place an upper limit on the reduction potential for $\mathbf{1^R}$. The strongest oxidant, $\mathbf{1^H}$, could readily oxidize a slight excess of ferrocene (~6 equiv added to a 6.7×10^{-5} M solution of $\mathbf{1^H}$); however, it was incapable of readily oxidizing substrates with higher one-electron oxidation potentials than ferrocene through an SET pathway. Complexes $\mathbf{1^{MeO}}$ and $\mathbf{1^{Me_2N}}$ required stronger reductants to facilitate their reductions, as no immediate reaction is observed when excess ferrocene is added to these solutions. Complex $\mathbf{1^{MeO}}$ was readily reduced by ethylferrocene, while $\mathbf{1^{Me_2N}}$ required dimethylferrocene as a reductant. Similar to results obtained with ferrocene and $\mathbf{1^{Me_2N}}$, ethylferrocene is incapable of reducing $\mathbf{1^{Me_2N}}$. These results strongly suggest that the trend in redox potentials follows the order $\mathbf{1^H} > \mathbf{1^{MeO}} > \mathbf{1^{Me_2N}}$, with an upper limit on the reduction potential of $\mathbf{1^{Me_2N}}$ being below 400 mV versus SCE (based on the CV data for $\mathbf{1^{MeO}}$). These results are in good agreement with those reported by Stack and co-workers, whom to our knowledge, are the only others to have reported estimates of reduction potentials involving Cu_2-O_2 species. Similar approaches were employed in those studies; approximate reduction potentials of Cu_2−dioxygen adducts centered about 500 mV versus SCE using decamethylferrocene as the reductant in redox titrations.[29,38]

Our EPR spectroscopic inquires (see Results) indicate that the ferrocene reductions of $[\{Cu^{II}(MePY2)^R\}_2(O_2^{2-})]^{2+}$ ($\mathbf{1^R}$) involve 2 equiv of ferrocene per Cu_2−dioxygen adduct. We suggest that following consumption of 1 equiv of the ferrocene, an unstable and spectroscopically undetectable $[Cu^{II}Cu^{III}(O)_2]^+$ species is formed (Scheme 5) that transforms through a disproportionation reaction to give 1 equiv of a "fully reduced" species and 1 equiv of $\mathbf{1^R}$. This makes the overall process appear as though it consumes 2 equiv of ferrocene derivative. There are two possible processes that may produce the fully reduced species, which could be the bis-μ-hydroxo dicopper(II) complexes $\mathbf{2^R}$ with protons which we presume derived from solvent. One is that the $Cu^{II}Cu^{III}$ mixed-valence one-electron-reduced product can readily and rapidly accept a second electron from a second equivlent of decamethylferrocene. Although possible, we think this situation to be unlikely as the formation of a $[Cu^{II}_2-O_2^{2-}]^0$ species from a stable $[Cu_2-(O_2^{2-})]^{2+}$ complex

should be thermodynamically unfavorable; no reduced Cu^{II}_2–bis-μ-oxo complex has ever been observed. The second possibility, as we suggested above as being more likely, is that the mixed-valence species is produced and undergoes a rapid disproportionation reaction. Furthermore, the CV studies on $\mathbf{1^R}$ indicate that they are unstable with respect to reduction by one electron even if no protons are present. It should also be pointed out that although a trimeric $Cu^{III}Cu^{II}_2-(O)_2$ species has been isolated,[41,80−82] a mixed-valence $Cu^{II}Cu^{III}-(O)_2$ complex has never been observed, suggesting that such species are highly unstable.

It appears that oxidations of substrates by one electron are aided by the thermodynamic driving force imparted by a proton transfer (PT) event. For example, all three complexes are incapable of oxidizing $[Fe^{II}(phen)_2(phen\text{-}NO_2)](ClO_4)_2$ ($E_{1/2}$ = 1.3 V versus SCE in CH_2Cl_2). No reaction is observed when a solution of $[Fe^{II}(phen)_2(phen\text{-}NO_2)](ClO_4)_2$ is injected into a solution of $\mathbf{1^R}$ at −80 °C. However, upon the addition of ammonium perfluorotetraphenylborate as a proton source, $[Fe^{II}(phen)_2(phen\text{-}NO_2)](ClO_4)_2$ is readily oxidized by all three $\mathbf{1^R}$, resulting in $\mathbf{2^R}$ as the sole copper-containing product. Overall, these results clearly indicate that $\mathbf{1^R}$ complexes are capable of oxidizing substrates with much less favorable ET driving forces through a PCET pathway. In other words, the availability of protons and PT makes the ET event thermodynamically favorable, driving the overall reaction to completion. This helps explain why substrates with E_{ox} much more positive than for $\mathbf{1^R}$ (>1.5 V; e.g., THF, Et_2O, and 4-CN-DMA)[44] can be readily oxidized by $\mathbf{1^R}$. In these reactions, a PT event following (or coupled to) the ET reaction can thermodynamically drive the reaction to completion. Similar results have been observed by Tolman and co-workers, who have seen that ferrocene is unreactive toward some tacn-ligated Cu_2-O_2 complexes unless an acid source is added.[31] This facilitated a redox reaction producing ferrocenium and reduced copper products.

If we now make the PT event less favorable by using a weaker acid (i.e., acetic acid, which is weaker than ammonium by ∼7 pK_a units in MeCN), then no reaction is observed between $[Fe^{II}(phen)_2(phen\text{-}NO_2)](ClO_4)_2$ and $\mathbf{1^R}$. This most likely results from a combination of the low driving force for ET ($[Fe^{II}(phen)_2(phen\text{-}NO_2)](ClO_4)_2$ is a weak reductant) coupled to the low driving force for protonation (acetic acid is a fairly weak acid in CH_2Cl_2); the resulting Cu_2-OOH adduct formed under these conditions would have a significantly weaker O−H bond than that which was formally "broken"; therefore, the overall reaction is not thermodynamically viable and will not proceed.[83] Attempts to estimate peroxo/bis-μ-oxo pK_as, which is vital to better estimate Cu_2-OOH BDEs for $\mathbf{1^R}$,[65] were not fruitful for three reasons. One is that $\mathbf{1^R}$ complexes are not very stable toward acid; over a relatively short period of time (minutes to hours), we observe the decomposition of $\mathbf{1^R}$ to $\mathbf{2^R}$, even after the addition of relatively weak acids. We believe that the autoreduction pathways of $\mathbf{1^R}$, mentioned above, are accelerated by acid sources. Therefore, photometric acid/base titrations would be exceptionally difficult. Another reason that pK_a estimations are impractical in the present system is that many of the weak acids that could be used, such as thiophenol or phenol, will also act as substrates to $\mathbf{1^R}$, giving up a formal H• to the copper complexes. A third and most important reason that a full pK_a study cannot be adequately performed is due to the lack of quantitative or meaningful data for pK_a's in CH_2Cl_2. Although the trend in acidity between MeCN and CH_2Cl_2 is similar,[84] exact values are not known. We can, therefore, only place a lower limit on the peroxo/bis-μ-oxo pK_a values for $\mathbf{1^R}$ in CH_2Cl_2 as being ∼15; however, the actual pK_as may be much larger in magnitude.

Similar to the observations noted by monitoring the reduction of $\mathbf{1^R}$ by decamethylferrocene, no mixed-valent copper species (i.e., EPR detectable copper species) are observed when substoichiometric amounts of TEMPO-H are added to $\mathbf{1^R}$, yet the full formation of TEMPO• is noted by spin integration (Scheme 4). Therefore, a $Cu^{II}Cu^{III}(O)(OH)^{2+}$ species, which may possibly have formed in such reactions, may be so unstable with respect to disproportionation that they are undetectable using these methods. This is supported by UV−vis titrations involving TEMPO-H, which afforded no detectable intermediate. Only the clean conversion of $[\{Cu^{II}(MePY2)^R\}_2(O_2)]^{2+}$ ($\mathbf{1^R}$) to $[\{Cu^{II}(MePY2)^R\}_2(OH)_2]^{2+}$ ($\mathbf{2^R}$) is observed. We should also note that if 1 equiv of $\mathbf{2^R}$ is added to a solution of $\mathbf{1^R}$, no observable reaction occurs, suggesting the mixed-valence complex is thermodynamically unstable with respect to the combination of $[\{Cu^{II}(MePY2)^R\}_2(O_2)]^{2+}$ ($\mathbf{1^R}$) and $[\{Cu^{II}(MePY2)^R\}_2(OH)_2]^{2+}$ ($\mathbf{2^R}$) (i.e., these two compounds do not comproportionate).

Substrate Coordination and Oxidation. The oxidation of THF by $\mathbf{1^{Me_2N}}$ has been studied by us and was shown to display second-order reaction kinetics behavior (first order in $\mathbf{1^{Me_2N}}$, first order in THF). The low activation enthalpy ($\Delta H^{\ddagger}$ = 3.7 kcal mol^{-1}) and large negative activation entropy ($\Delta S^{\ddagger}$ = −56 cal mol^{-1} K^{-1}) (see Supporting Information) for this reaction suggest a pre-equilibrium THF binding step followed by oxidation; however, saturation behavior was not observed. Furthermore, reactions with $\mathbf{1^{MeO}}$/$\mathbf{1^H}$ and THF suggested that as little as 1 equiv of MeCN (as a competitive inhibitor) could dramatically influence the observed second-order rate constant, which lends more evidence to a substrate coordination event. In contrast to THF oxidation, variable temperature kinetic studies of DMA oxidation by $\mathbf{1^R}$ *does* provide clear evidence that oxidation takes place following DMA binding to the metal complex. At high DMA concentration (>20 mM), the observed rate constant begins to plateau, clearly demonstrating saturation behavior (i.e., substrate coordination; see Figure 2). This is strongly pronounced at low temperatures (i.e., <−70 °C).

The quality of the fits to the data and narrow temperature range necessitated by the stability of $\mathbf{1^R}$ makes it difficult to draw any detailed conclusions concerning the thermodynamic and kinetic properties of the $\mathbf{1^R}$ series, yet generalizations can be reached. One is that binding of DMA to the metal center appears to be entropically controlled, as may be expected. The calculated $\Delta S°$ values for DMA binding are all <−40 cal mol^{-1} K^{-1}, which is in line with the need to use low temperatures

(79) Addison, A. W.; Rao, T. N.; Reedijk, J.; van Rijn, J.; Verschoor, G. C. *J. Chem. Soc., Dalton Trans.* **1984**, 1349−1356.
(80) Machonkin, T. E.; Mukherjee, P.; Henson, M. J.; Stack, T. D. P.; Solomon, E. I. *Inorg. Chim. Acta* **2002**, *341*, 39−44.
(81) Cole, A. P.; Root, D. E.; Mukherjee, P.; Solomon, E. I.; Stack, T. D. P. *Science* **1996**, *273*, 1848−1850.
(82) Root, D. E.; Henson, M. J.; Machonkin, T.; Mukherjee, P.; Stack, T. D. P.; Solomon, E. I. *J. Am. Chem. Soc.* **1998**, *120*, 4982−4990.
(83) (a) Mayer, J. M. *Acc. Chem. Res.* **1998**, *31*, 441−450. (b) Roth, J. P.; Yoder, J. C.; Won, T.-J.; Mayer, J. M. *Science* **2001**, *294*, 2524−2526.
(84) Kim, H.-s.; Chung, T. D.; Kim, H. *J. Electroanal. Chem.* **2001**, *498*, 209−215.

(<−70 °C) to observe clear evidence of DMA coordination to **1**$^{\mathbf{R}}$. In contrast, the calculated $\Delta H°$ values appear to favor DMA binding by ∼10 kcal mol^{-1}. Once binding occurs, the oxidation reactions are driven by fairly low $\Delta H^{\ddagger}$, which were all under 15 kcal mol^{-1}. Although these activation enthalpies are lower than those typically observed for metal-mediated PCET reactions,[83a] they are not without precedent. For example, intramolecular N-dealkylations by Cu^{III}_2−bis-μ-oxo complexes reported by Itoh and co-workers proceed with $\Delta H^{\ddagger}$ well below 10 kcal mol^{-1}.[9]

It was noted above that substrate oxidation rates as a function of R (for **1**$^{\mathbf{R}}$) appear to be the opposite of what one may expect. The *weakest* SET oxidant affords the fastest reaction rates, while the *strongest* SET oxidant affords the slowest oxidation rates! This can be the result of many different factors, including stronger hydroxo O−*H* bond strengths in the product **2**$^{\mathbf{Me_2N}}$ compared to those in **2**$^{\mathbf{H}}$, differing amounts of Cu^{III}_2−bis-μ-oxo isomer in the **1**$^{\mathbf{R}}$ series, or different ligand coordination environments about the metal center (vide infra). All three could have a dramatic influence on the oxidation rates of these PCET reactions, and unfortunately, we do not see ways of sorting out how these (or other) factors may be influencing reactivity with this system.

Substrate coordination to the metal center prior to oxidation reactions has been observed via kinetic studies by Itoh for phenolate *ortho* hydroxylations.[18] There, the presence of an anionic phenolate aids in coordination to the metal center, and relatively weak binding occurs, $K_{eq} \sim 500-1000$ M^{-1},[18] which compares well with our results.[86] In a related trinuclear Cu_3-O_2 system,[40] there is evidence for phenol coordination prior to oxidation and corresponding *ortho* C−C coupling. There, substrate binding is much weaker ($K = 44.6(22)$ M^{-1}) even at low temperatures (203 K).[40] Furthermore, the majority of known oxidation reactions involving discrete Cu_2-O_2 complexes involve ligand oxidative N-dealkylations.[9] In all of these cases, the "substrate" is already coordinated to the metal center, negating the binding step.

All of these findings suggest why thermodynamic considerations could not predict that DHA, Me_2THF, and toluene (all with weaker X−H bonds) would not be oxidized by **1**$^{\mathbf{R}}$. It appears that a substrate coordination event must take place prior to oxidation by **1**$^{\mathbf{R}}$, but these substrates would be (mostly) incapable of coordinating to the metal complex. DHA and toluene are hydrocarbons with no heteroatom Lewis base to facilitate coordination to the copper complex oxidants, while the ether oxygen atom in Me_2THF is rather sterically inaccessible compared to its counterpart in the unsubstituted THF substrate. It should be pointed out that DHA oxidation (and lack thereof) by Cu_2-O_2 complexes is not well understood. Work by Stack and co-workers is consistent with our studies where some Cu^{III}_2−bis-μ-oxo systems do not appear to react with DHA.[38] This is despite the fact that these complexes will oxidize substrates with much stronger X−H bonds, all of which happen to contain a heteroatom that is sterically accessible to the metal center. By contrast, Itoh's Cu^{III}_2−bis-μ-oxo species *is* reported to react with DHA as well as the structurally related compound, 10-methyl-9,10-dihydroacridine (MDA).[30] Kinetic analysis of MDA oxidation suggests an apparent third-order reaction (first order in MDA, second order in Cu^{III}_2−bis-μ-oxo), the mechanistic implications of which are ambiguous at this time.

ETPT versus ET/PT using Mechanistic Probes. Oxidation of CMA by $[\{Cu^{II}(MePY2)^{R}\}_2(O_2)]^{2+}$ (**1**$^{\mathbf{R}}$) results in the formation of bis-μ-dihydroxy−dicopper(II) complexes, **2**$^{\mathbf{R}}$ (Scheme 3), as the sole isolable copper-containing products. CMA oxidations by **1**$^{\mathbf{MeO}}$ and **1**$^{\mathbf{H}}$ will be discussed first. Here, GC/MS analysis revealed a number of different organic products in the reaction. The major product, in fact, is *N*-methylaniline (MA), comprising the majority of the resulting oxidation product mixture, strongly supporting the conclusion that an ET/PT pathway occurs (Schemes 7 and 10).

If an ETPT event occurred, then *N*-methyl dealkylation is preferred due to steric, statistical, and thermodynamic reasons. Therefore, *N*-cyclopropylaniline (CA) should be the major oxidation product under ETPT conditions. We do find that CA is formed in both reactions; however, its contribution to the overall oxidation product mixture is less than 6% in both cases, which lends additional evidence that a rate-limiting ET/PT pathway is occurring during the oxidation of CMA. A third product is also observed, which we tentatively assign as the ring-opening product, PMA, although we should point out that definitive proof (i.e., comparison with an authentic standard) as to its identity is lacking.[77] Formation of PMA is supported by mass spectrometry ($m/z = 163.1$) and makes mechanistic sense if we consider the following scenario. SET (the first step in the ET/PT scheme) would lead to an initially formed *N*-cyclopropyl radical cation, unstable with respect to very rapid ring opening, $k > 10^8$ s^{-1} at −80 °C.[87] This radical center could then couple to the phenyl ring *ortho* to the amine moiety. The unstable radical cation will then rapidly lose a proton, forming intermediate MQ$^{\bullet}$, which has a radical center α to the amine group. This can then undergo a "rebound" step, capturing an HO$^{\bullet}$ from the $Cu^{II}OHCu^{III}O$ intermediate. Hydroxyl radical capture by a structurally related amine radical, which forms an α-amino alcohol, has been previously observed in photolysis experiments.[79] Hydroxyl group capture during a rebound step is also supported by DMA and THF oxidation by **1**$^{\mathbf{R}}$.[42] The α-amino alcohol formed from MQ$^{\bullet}$ can then undergo a rapid ring-opening reaction, forming aldehyde PMA (see Scheme 10), which would be in equilibrium with different iminium salts formed through both inter- and intramolecular Schiff base condensations. Iminium salt formation from PMA was indicated by our attempted synthesis of PMA, which demonstrated that PMA rapidly polymerizes; authentic PMA rapidly turns into brown, sticky, insoluble polymers.[77]

The oxidation of CMA by **1**$^{\mathbf{Me_2N}}$ yields a distinctly different product distribution, yet still supports the ET/PT mechanism of reaction. First, almost no MA is observed. In fact, virtually no organic products can be observed in the GC trace. Instead, what is isolated from the reaction is *N*-methylquinolinium (MQ^+) (Scheme 10). This product has been previously identified in heme−oxygenase oxidations of CMA and is readily formed

(85) Itoh, S.; Kumei, H.; Taki, M.; Nagatomo, S.; Kitagawa, T.; Fukuzumi, S. *J. Am. Chem. Soc.* **2001**, *123*, 6708−6709.

(86) The phenolate oxidations reported by Itoh were carried out in acetone. This solvent may compete somewhat with phenolate coordination, which could suppress phenolate binding constants in this system.

(87) The reported rate constant for ring opening of a *N*-methyl-*N*-(*trans*-2-phenylcyclopropyl)aminyl radical (a structurally related compound to CMA) has been measured at 7.2×10^{11} s^{-1}: Musa, O. M.; Horner, J. H.; Shahin, H.; Newcomb, M. *J. Am. Chem. Soc.* **1996**, *118*, 3862−3868. Our estimate of the lower limit for ring opening of CMA^+ comes from this value and then extrapolating down to −80 °C using the Arrhenius equation: $k = Ae^{-E_a/RT}$.

Scheme 10

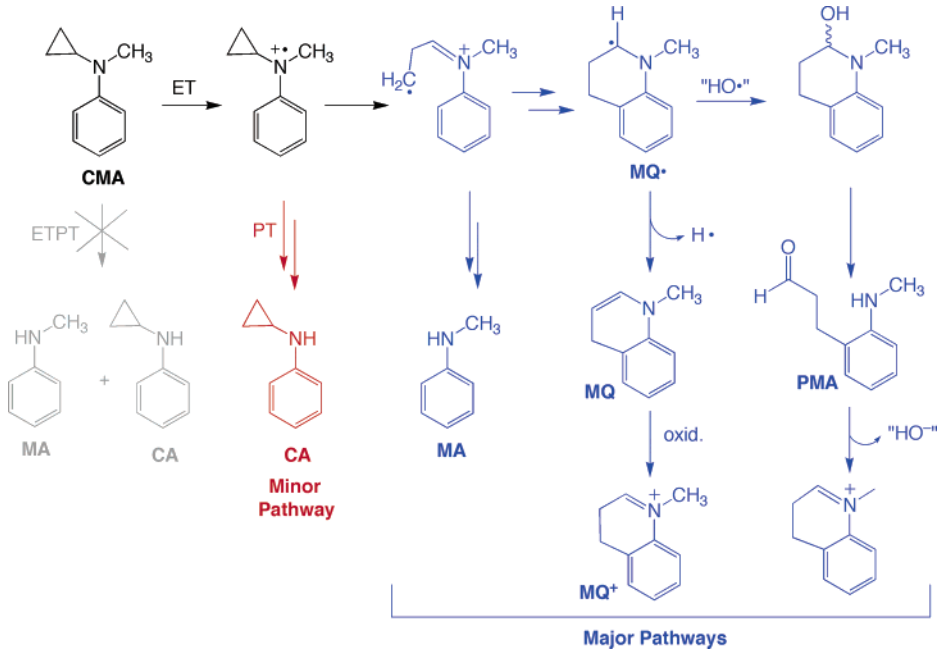

from $MQ^{\bullet}$.[47,88] If the rebound step is sufficiently slow with respect to a second ET/PT reaction, then a second $H^{\bullet}$ loss is observed instead of $HO^{\bullet}$ capture. As indicated above in the EPR studies, the mixed-valence forms of $\mathbf{1^R}$ are very unstable with respect to abstracting a second $H^{\bullet}$. It has been previously[42] demonstrated that $\mathbf{1^{Me_2N}}$ is particularly reactive compared to $\mathbf{1^H}$ and $\mathbf{1^{MeO}}$ and, therefore, may abstract a second H• more quickly than $\mathbf{1^H}$ or $\mathbf{1^{MeO}}$. Loss of $H^{\bullet}$ results in 2-dihydro-*N*-methylquinoline (MQ), which rapidly oxidizes upon exposure to O_2 (or to a second equivalent of $\mathbf{1^{Me_2N}}$), forming MQ^+ (see Scheme 9). Due to the inherently unstable nature of MQ, its direct observation has thus far been elusive, but can be inferred from the formation of MQ^+. As a result of the cationic nature of MQ^+ and the small reaction scales necessitated for experimental reasons, quantification of reaction yields between $\mathbf{1^{Me_2N}}$ and CMA was extremely difficult. Therefore, we could estimate a lower limit on the yield of MQ^+ (MQ) based on a gravimetric analysis of the recovered product at ~50%, which assumes a two-electron oxidation of CMA to MQ followed by the air oxidation of MQ to MQ^+. It is also plausible that the oxidation of CMA to MQ^+ does not require O_2 and is produced directly in the solution (i.e., the 2 e^- oxidation of CMA to MQ by 1 equiv of $\mathbf{1^{Me_2N}}$ would be rapidly followed by another equivalent of $\mathbf{1^{Me_2N}}$ oxidizing MQ to MQ^+), which would make this oxidation a near quantitative process. This would be in line with the fact that no MQ is observed, even during anaerobic workup of the reaction. Such a scenario is also consistent with the unstable nature of $\mathbf{1^{Me_2N}}$ with respect to reducing conditions.

Thus, in all three cases, it appears that $[\{Cu^{II}(MePY2)^R\}_2(O_2)]^{2+}$ ($\mathbf{1^R}$) oxidizes CMA via an ET/PT pathway (vide supra). This is despite the fact that the one-electron oxidation of CMA is thermodynamically unfavorable by approximately $^1/_2$ V. Coupling in the protonation step (PT) makes the overall oxidation favorable, as indicated by the acid−base/redox titrations mentioned above. This type of mechanism is supported by the vast body of work concerning coupled versus uncoupled metal-mediated PT and ET reactions.

Benzylic alcohol MDP is also oxidized by $[\{Cu^{II}(MePY2)^R\}_2(O_2)]^{2+}$ ($\mathbf{1^R}$) (Scheme 8); however, these reactions are all considerably slower than those between $\mathbf{1^R}$ and CMA, taking days to go to completion. This could be due to either a change in the thermodynamic driving force of the reaction (MDP is 1.0 V less reducing) *or* potential differences in rates between ETPT and ET/PT, which can both dramatically influence reaction rates. Differences in oxidation rates could also be due to the increased steric bulk of MDP compared to that of CMA, which may limit its access to the metal complex. Considering that substrate coordination to the metal center seems to be a requirement for oxidation activity, this seems to be a reasonable supposition (vide supra).

In the case of $\mathbf{1^{MeO}}$ and $\mathbf{1^{Me_2N}}$ oxidation of MDP, the sole isolable organic product is ketone MDK (Scheme 8). This is strong evidence in favor of an ETPT reaction, in contrast to the ET/PT oxidation of CMA facilitated by these complexes. In an ET/PT scheme, oxidation of MDP will form a charged radical cation intermediate, which will rapidly lead to $\alpha-\beta$ C−C bond cleavage and result in MBA. However, ETPT reactions would result in a relatively stable neutral radical species, which would simply lose an additional hydrogen atom to form MDK. The change in mechanism between CMA (see above) and MDP oxidations by $\mathbf{1^{MeO}}$ and $\mathbf{1^{Me_2N}}$ can be largely explained by the fact that MDP is roughly 1.0 V harder to oxidize by one-electron than is CMA, yet both CMA and MDK have similar C−*H* BDEs (~85 kcal mol^{-1}). Therefore, the overall MDK oxidation would still be thermodynamically viable, and the ETPT pathway may be the more easily accessible pathway (i.e., compare to ET/PT) for $\mathbf{1^{MeO}}$ and $\mathbf{1^{Me_2N}}$ oxidations, with substrates possessing such inaccessible oxidation potentials and "weak" X−H bonds. This is supported by our previous study investigating *para*-substituted dimethylaniline (R-DMA) oxidations by $\mathbf{1^R}$.[44] There, we found that as the R-DMA was made more difficult to oxidize, the mechanism switched over from ET/PT to ETPT. Switching

(88) Shaffer, C. L.; Morton, M. D.; Hanzlik, R. P. *J. Am. Chem. Soc.* **2001**, *123*, 8502−8508.

mechanisms between ET/PT and ETPT as the substrate is made more difficult to oxidize has been observed in a wide variety of metal−oxo-mediated substrate oxidations. Most notable are high-valent Fe−oxo porphyrinates,[89,90] which will perform both ETPT *and* ET/PT reactions depending on the oxidation potential of the substrate.

In contrast, $[\{Cu^{II}(MePY2)^{H}\}_2(O_2)]^{2+}$ (**1**$^{\mathbf{H}}$) can oxidize MDP in a different manner, mostly through an ET/PT pathway, as indicated by formation of MBA as the major oxidation product (Scheme 8). This is also supported by our previous R-DMA study, which demonstrated that only an ET/PT pathway is operable for **1**$^{\mathbf{H}}$ oxidations.[44] Surprisingly, we also found that approximately $^1/_3$ of the MDP can be oxidized via the ETPT pathway, as indicated by the formation of ketone MDK as the minor product. This was not hinted at in the previous 4-substituted 4-R-DMA studies,[44] probably due to the ambiguity in interpreting kinetic isotope effect data.

In previous work, Baciocchi[46] and Mayer[91] utilized MDP as a probe for metal−oxo-mediated oxidation reactions. Mayer and co-workers have shown that MDP oxidation by $Mn(hfacac)_3$ proceeds through an ET/PT pathway, which may be expected given that $Mn(hfacac)_3$ is significantly more oxidizing than **1**$^{\mathbf{R}}$. In this case, MDP SET would be thermodynamically downhill and, therefore, accessible.[91] Baciocchi has shown that Co^{III}−W in acidic aqueous solutions also results in an ET/PT oxidation chemistry, while cytochrome P450 (which contains a $[(por^{+\bullet})$-$Fe^{IV}{=}O]$ moiety in its active form) will oxidize MDP through an ETPT pathway.[48]

Differential Reactivity and Relation to Copper Catalysis. The difference in oxidative reactivity of $[\{Cu^{II}(MePY2)^{H}\}_2$-$(O_2)]^{2+}$ (**1**$^{\mathbf{H}}$) versus **1**$^{\mathbf{MeO}}$/**1**$^{\mathbf{Me_2N}}$ toward MDP, DMA, and CMA could be the result of several different factors. One could be a difference in substrate approach to the metal center. We have evidence from the crystal structures of **2**$^{\mathbf{R}}$ that the ligand adopts different geometries about the metal center of these μ-hydroxo complexes (see discussion above, and Scheme 9). A similar trend may exist for Cu_2O_2 complexes **1**$^{\mathbf{R}}$. Further support for differential ligand coordination environments in **1**$^{\mathbf{MeO}}$/**1**$^{\mathbf{Me_2N}}$ versus **1**$^{\mathbf{H}}$ comes from resonance Raman spectroscopic studies and vibrational analyses of **1**$^{\mathbf{R}}$.[43] The $Cu-N_{py}$ stretching frequencies are measurably higher in peroxo complexes **1**$^{\mathbf{MeO}}$ and **1**$^{\mathbf{Me_2N}}$ (295 and 305 cm^{-1}, respectively) compared to that in **1**$^{\mathbf{R}}$ (275 cm^{-1});[43] as the N donor strength of pyridine is increased, the copper ion moves more into plane and the tertiary nitrogen and oxygen ligands become poorer donors. Additional precedent for the current suppositions concerning **1**$^{\mathbf{H}}$/**2**$^{\mathbf{H}}$ comparisons comes from Tolman and co-workers,[92] who have published crystallographic evidence that a similar ligand coordination environment (i.e., wrapping of the multidentate nitrogenous ligand about Cu) exists for both $Cu^{III}_2-(O^{2-})_2$ and $Cu^{II}_2-(OH)_2$ complexes. If the coordination environment is similar in the peroxo and bis-μ-oxo cases, then the substrate may have differential binding geometries in **1**$^{\mathbf{H}}$ versus **1**$^{\mathbf{MeO}}$/**1**$^{\mathbf{Me_2N}}$, which may make the ETPT pathway less favorable in **1**$^{\mathbf{H}}$ due to geometric constraints and a diminishing likelihood

Scheme 11

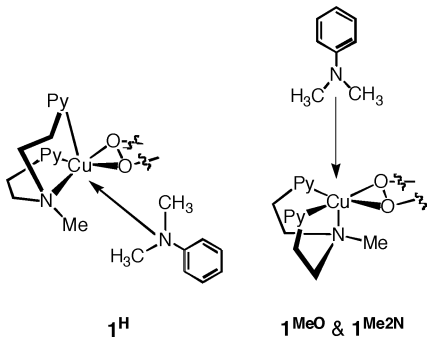

that an oxygen atom derived $H^{\bullet}$ or H^+ acceptor would lie proximate to the bound substrate. Also, differential substrate binding patterns could hinder the substrate from approaching the metal center in **1**$^{\mathbf{H}}$ versus **1**$^{\mathbf{MeO}}$ and **1**$^{\mathbf{Me_2N}}$, which can have a dramatic influence on reaction rates and pathways (see Scheme 11).

Another reason for the differential reactivity between **1**$^{\mathbf{H}}$ versus **1**$^{\mathbf{MeO}}$/**1**$^{\mathbf{Me_2N}}$ may be the consequence of varying amounts of peroxo/bis-μ-oxo isomer in solution. Complex **1**$^{\mathbf{H}}$ is almost all peroxo (∼90:10 peroxo:bis-μ-oxo), while **1**$^{\mathbf{Me_2N}}$ and **1**$^{\mathbf{MeO}}$ have substantially more bis-μ-oxo isomer present (∼75:25 peroxo:bis-μ-oxo).[43] It is possible that the bis-μ-oxo isomer is responsible for the ETPT pathway, as is suggested by the many examples of $H^{\bullet}$ abstraction chemistry by bis-μ-oxo dicopper(III) complexes[9] and from computational results.[6,7,93] These molecular orbital (MO) calculations have suggested that the peroxo tautomer is incapable of facilitating ETPT reactions, however, would be capable of facilitating ET/PT (and hydride transfer) reaction. In contrast, MO calculations seem to support the idea that the bis-μ-oxo tautomer is capable of supporting ETPT reactions; however, its ET ability has not been probed, and in the end, it may prove to be a more capable SET oxidant than the peroxo tautomer. Therefore, it seems reasonable that the complex with the most bis-μ-oxo isomer present would be more likely to undergo an ETPT reaction, while the peroxo isomer may be responsible for the ET/PT reaction. This could explain why both ETPT and ET/PT pathways are operable for MDP oxidation by **1**$^{\mathbf{H}}$; however, it alone cannot explain why there is no ET/PT product observed for MDP oxidation by **1**$^{\mathbf{MeO}}$ and **1**$^{\mathbf{Me_2N}}$.

It should be pointed out that at this point we *cannot* state which tautomer (peroxo, bis-μ-oxo, or both) is responsible for the observed reactivity. However, it is quite interesting that the complex that contains the most bis-μ-oxo tautomer (**1**$^{\mathbf{Me_2N}}$) is the "best" oxidant in terms of both the fastest reaction rates and the highest yields of product. Whether this is merely a coincidence or suggestive that the bis-μ-oxo tautomer is the reactive species remains to be seen. Furthermore, $[\{Cu^{II}$-$(MePY2)^{Me_2N}\}_2(O_2)]^{2+}$ (**1**$^{\mathbf{Me_2N}}$) is also the complex that is the weakest SET oxidant, which means that other factors (possibly differing bis-μ-oxo complex acidities)[94] *must* be playing a significant role in these oxidations.

(89) Sato, H.; Guengerich, F. P. *J. Am. Chem. Soc.* **2000**, *122*, 8099−8100.
(90) Hall, L. R.; Hanzlik, R. P. *J. Biol. Chem.* **1990**, *265*, 12349−12355.
(91) Bryant, J. R.; Taves, J. E.; Mayer, J. M. *Inorg. Chem.* **2002**, *41*, 2769−2776.
(92) Mahapatra, S.; Halfen, J. A.; Wilkinson, E. C.; Pan, G.; Wang, X.; Young, V. G., Jr.; Cramer, C. J.; Que, L., Jr.; Tolman, W. B. *J. Am. Chem. Soc.* **1996**, *118*, 11555−11574.
(93) Henson, M. J.; Mukherjee, P.; Root, D. E.; Stack, T. D. P.; Solomon, E. I. *J. Am. Chem. Soc.* **1999**, *121*, 10332−10345.
(94) We suggest that bis-μ-oxo complex $[\{Cu^{III}_2(MePY2)^{Me_2N}(O)_2]^{2+}$, because of its Me_2N ligand substituents and resulting coordination properties, may form a stronger O−H bond upon acceptance of H^+ or $H^{\bullet}$ from a substrate, explaining the enhanced reactivity of **2**$^{\mathbf{Me_2N}}$.

More broadly, the results presented here seem to suggest that oxidations by catechol oxidase (CO) probably occur through a PCET pathway. If analogies are to be made between these copper complexes and the active site of CO, it seems reasonable to suggest that the Cu_2-O_2 center is a weak one-electron oxidant and may need to make use of a PT event following ET to thermodynamically drive the oxidation of catechols to *ortho*-quinones to completion. A major facet of the research presented above suggested that substrate coordination to the metal centers is a major factor in substrate oxidations. Substrate coordination has been suggested to take place in both CO and Tyr, which this study (and those from Itoh)[18,40] fully supports. Therefore, if Cu_2-O_2 species were to be used in synthetic and catalytic systems to promote practical oxidation reactions, it may be prudent to design ligands in such a way that the copper center would be accessible to the substrate. Also, these studies suggest that a strong SET reagent is not necessary to promote these PCET oxidations if the overall thermodynamics of the PCET reactions are favorable.

Summary and Concluding Remarks

In this study, we have attempted to provide a more in-depth understanding of the initial steps of the oxidation of substrates by $[\{Cu^{II}(MePY2)^{R}\}_2(O_2)](B(C_6F_5)_4)_2$ (**1**$^{\mathbf{R}}$). We have provided clear evidence for substrate coordination to the metal complex, most likely at one of the two copper centers; this is vital for subsequent oxidation reactions to take place. Furthermore, as a new approach to studies in copper−dioxygen substrate oxidation chemistry, we have used mechanistic probes to show that these complexes are capable of oxidizing substrates through both ETPT and ET/PT reactions. Complexes **1**$^{\mathbf{R}}$ appear to be moderately to weakly oxidizing, and the SET oxidation reactions of all of the substrates investigated are certainly thermodynamically uphill processes. Therefore, **1**$^{\mathbf{R}}$ makes use of PCET pathways to effect substrate oxidations/oxygenations. At moderately unfavorable thermodynamic driving forces for electron transfer from substrate to **1**$^{\mathbf{R}}$, it appears that an ET/PT process is dominant. At very unfavorable thermodynamic driving forces, the ETPT process is foremost. These results are summarized in Scheme 12. A switchover in mechanism has also been observed in other metal-mediated oxidations as a function of substrate oxidation potential.[44,91] We must qualify these concluding statements by pointing out that since we implicate DMA, THF, or other substrate binding to the copper−dioxygen complexes, reference to ET processes may be better described as "inner-sphere substrate electron-transfer" oxidations; nevertheless, clear mechanistic differentiation based on established ETPT versus ET/PT mechanistic criteria is observed here in these **1**$^{\mathbf{R}}$-mediated substrate oxidations. Investigations on other systems are needed to determine if the findings here are general and also to provide a more comprehensive understanding of copper−dioxygen substrate reactivity patterns and mechanism of action.

Scheme 12

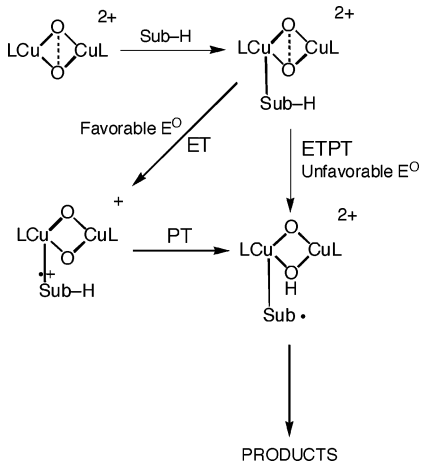

Acknowledgment. This work was supported by a grant from the National Institutes of Health (K.D.K., GM28962), and a Public Health Service Postdoctoral Fellowship (J.S., F32GM067447).

Supporting Information Available: Plots of the temperature dependence of k_{obs} versus [DMA] for DMA oxidation of **1**$^{\mathbf{R}}$, temperature dependence of k_{obs} versus [THF] for THF oxidation by **1**$^{\mathbf{Me_2N}}$, van't Hoff and Eyring plots for DMA binding and oxidation by **1**$^{\mathbf{R}}$, CV data for **1**$^{\mathbf{Me_2N}}$, representative UV−vis of ferrocene "titrations" by **1**$^{\mathbf{H}}$ and **1**$^{\mathbf{Me_2N}}$, representative GCs for **1**$^{\mathbf{R}}$ oxidation of CMA, and cif files for X-ray structures of **2**$^{\mathbf{MeO}}$ and **2**$^{\mathbf{Me_2N}}$. This material is available free of charge via the Internet at http://pubs.acs.org.

JA045191A